Received: 23 June 2025 | Revised: 11 September 2025 | Accepted: 28 September 2025 | Published online: 17 November 2025

RESEARCH ARTICLE

Remote Sensing for Sustainable Oceans
2025, Vol. 00(00) 1-24
DOI: 10.47852/bonviewRSSO52026547

BON VIEW PUBLISHING

Spatiotemporal Variations and Trends of Atmospheric Parameters Influencing Coastal Resilience in Cox's Bazar, Bangladesh

Siraj Uddin Md Babar Chowdhury[1,*], Anik Karmakar[2], K. M. Azam Chowdhury[3], Tabassum Hossain Tahsin[2], Abdullah Al Mamun Siddiqui[1], Tasin Sumaia Khan[4], and Mohammad Rokan Uddin[2]

[1] *Bangladesh Oceanographic Research Institute, Bangladesh*

[2] *Department of Oceanography, University of Chittagong, Bangladesh*

[3] *Department of Oceanography, University of Dhaka, Bangladesh*

[4] *Department of Hydrography and Oceanography, Bangladesh Maritime University, Bangladesh*

Abstract: Cox's Bazar, located on the southeastern coast of Bangladesh, is highly exposed to the impacts of climate change due to its position along the Bay of Bengal. This region's high dependence on sectors such as fishing, agriculture, and tourism amplifies the research intent. The present study examines changes in major weather variables, including air temperature, surface pressure, relative humidity, wind speed and direction, and precipitation, over the period 2015–2024. High-resolution reanalysis datasets, along with in situ observations, were utilized to examine monthly, seasonal, and interannual variability and assess their influence on local ecosystems, livelihoods, and infrastructure. Empirical orthogonal function (EOF) analysis shows that the first principal component (PC1) explains 99% of the total variance, reflecting a strong annual cycle driven by the monsoon. Average temperatures increased steadily from 22.5°C in 2015 to approximately 24.0°C in 2024. Humidity also increased, reaching 78.45% by 2024, whereas the previous was 77.95% in 2015. Wind speeds fluctuated seasonally, averaging 4.1 m/s in spring and peaking at 5.1 m/s in May. Precipitation varied widely, with annual totals reaching 2791.4 mm in 2024. Changes indicate more intense weather events and shifting rainfall patterns, increasing the risks of flooding, erosion, and stress on local resources. Variations in wind also highlight the potential for wind energy development. The findings underscore the critical need for adaptive coastal management that considers climate trends, ecosystem health, and community preparedness. Such insights provide a basis for guiding policies to protect livelihoods and improve long-term resilience in this vulnerable coastal region.

Keywords: spatiotemporal variation, coastal zone management, weather variability, climate resilience, renewable energy potential

1. Introduction

Cox's Bazar, the world's longest natural sandy coastline and diverse coastal ecosystems, is one of Bangladesh's most climate-exposed regions [1]. Being located near the Bay of Bengal (BoB), it is highly vulnerable to the impacts of climate change. Rising sea levels, intense tropical cyclones, and frequent seasonal floods pose significant risks, particularly to communities dependent on fisheries, agriculture, and tourism [1, 2]. The low-lying nature of the coast makes the area highly vulnerable to climate variability, emphasizing the importance of effective management to protect both livelihoods and ecosystems [2]. Understanding the spatiotemporal dynamics of key weather parameters such as air temperature, surface pressure, humidity, wind speed, and precipitation is critical for understanding climate scenarios and developing strategies to mitigate related risks. Accurate and reliable weather data enhance forecasting and disaster preparedness, both of which are essential in this hazard-prone region [3]. Furthermore, the region's wind energy potential offers a pathway to improve energy security while addressing climate challenges [4].

***Corresponding author:** Siraj Uddin Md Babar Chowdhury, Bangladesh Oceanographic Research Institute, Bangladesh. Email: babar@bori.gov.bd

The Cox's Bazar–Teknaf coastal belt, stretching nearly 80 km along southeastern Bangladesh, lies between 20.34°N–21.35°N latitude and 91.50°E–92.23°E longitude. It is bordered by the BoB to the west and Myanmar to the southeast (Figure 1) [5]. Cox's Bazar, known for having the world's longest uninterrupted natural beach, serves as a major tourism center, and Teknaf marks the country's southernmost point at the mouth of the Naf River [6]. The region contains sandy beaches, mangroves, hill ranges, and estuaries [3], forming a sensitive coastal environment that is often affected by tropical cyclones and seasonal monsoons [1, 7, 8].

This study provides an elaborated spatiotemporal assessment of the historical and present weather patterns in Cox's Bazar, with a focus on their implications for coastal management [2, 9]. Outcomes deliver important insights for decision-makers and stakeholders, emphasizing the need for adaptive strategies that enhance the sustainability and resilience of coastal communities. By clarifying the long-term impacts of climate variability, this study supports improved planning, disaster preparedness, and resource management in one of Bangladesh's most vulnerable coastal regions [10, 11].

To achieve this, weather variability across the Cox's Bazar–Teknaf coastal belt was analyzed using a geographic grid system based on scale and compass orientation. Empirical orthogonal function (EOF) analysis identified the dominant modes of variability, and

Figure 1
Study area map of Cox's Bazar–Teknaf, Bangladesh, depicting major locations, including beaches and weather stations

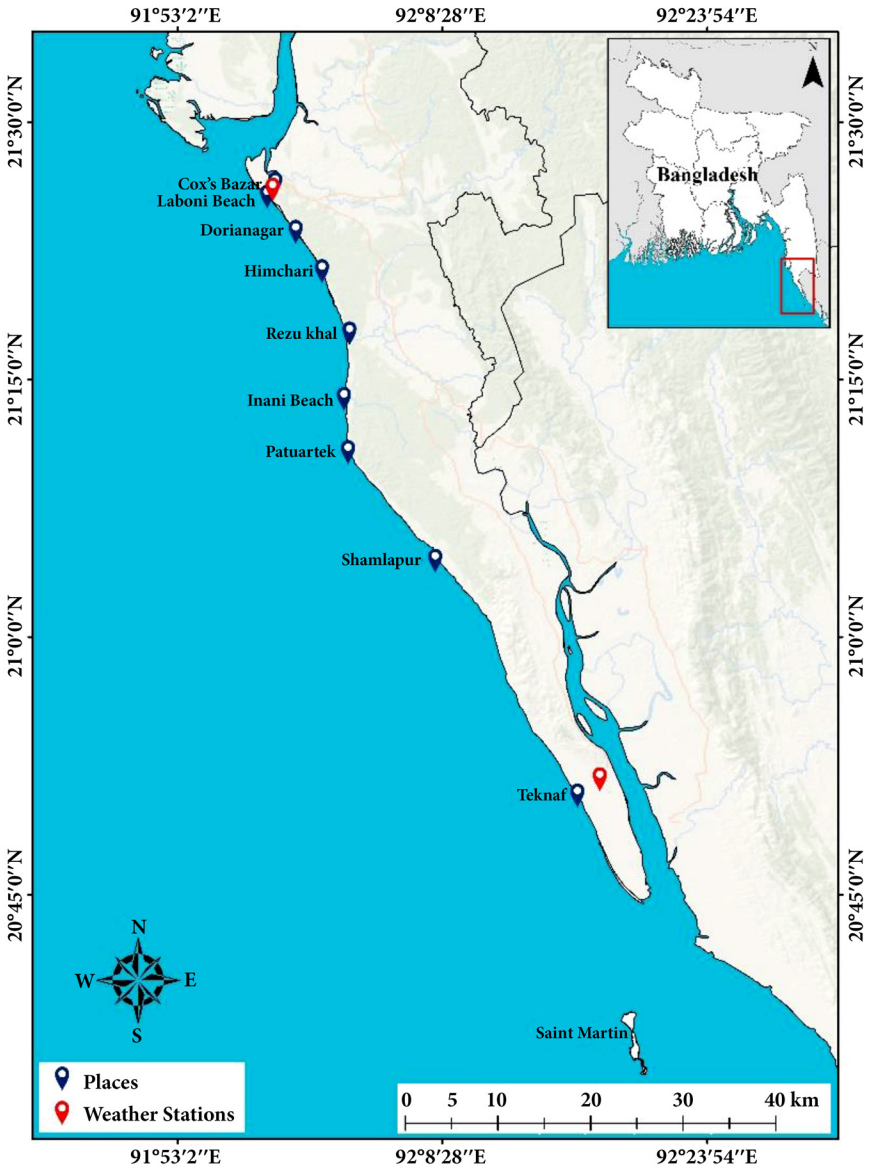

correlation and regression methods quantified relationships among climate variables, providing a clearer picture of seasonal trends and interdependent dynamics [12].

Despite growing research on climate variability in the BoB, there is a notable research gap regarding continuous, high-resolution, multiparameter analyses specifically focused on the Cox's Bazar–Teknaf coastal region. Few investigations link multiparameter weather variability with coastal resilience, disaster preparedness, or renewable energy prospects. Furthermore, the linkage between detailed weather variability and practical coastal zone management strategies, including disaster preparedness and renewable energy potential, remains underexplored.

This study addresses the research gap by combining EOF analysis with correlation, regression, and trend significance testing. The results highlight the main modes of variability and the interconnections among key weather parameters. These findings provide location-specific evidence that can guide adaptive coastal management, strengthen disaster preparedness, and promote sustainable development. By delivering statistically reliable insights, this study contributes both to academic understanding and to practical strategies for improving resilience in this climate-vulnerable coastal region [2, 9–11].

2. Data and Methods

2.1. Data sources

This study utilized diverse in situ and reanalysis datasets from January 2015 to December 2024 for analyzing weather impacts in Southeast Bangladesh. Air temperature, atmospheric pressure, relative humidity, and precipitation data were obtained from the CDS-ERA5[1] reanalysis product with a 0.25° × 0.25° spatial resolution. Wind data, including u- and v-components at a 10-m level, were also sourced from ERA5 hourly data on single levels[2] with the same resolution. In addition, monthly and annual averages of dry-bulb temperature, sea level pressure, total rainfall, relative humidity, and wind speed were

[1] Copernicus Climate Data Store – ERA5 reanalysis datasets: https://cds.climate.copernicus.eu/datasets

[2] ERA5 hourly data on single levels: https://cds.climate.copernicus.eu/datasets

incorporated from the Bangladesh Meteorological Department (BMD),[3] specifically from two weather stations located at Cox's Bazar (Laboni beach) (21.43°N, 91.97°E) and Teknaf (20.86°N, 92.30°E), to ensure the validity of the analysis.

2.2. Methods

This study applied a combination of observational data, reanalysis products, and statistical methods to investigate weather variability in the Cox's Bazar–Teknaf coastal region. High-resolution datasets were obtained from the Climate Data Store and the BMD. ERA5 reanalysis data were used at their sourced spatial resolution of 0.25° × 0.25°, alongside in situ station records from Cox's Bazar and Teknaf provided in CSV format. Key variables, including air temperature, humidity, atmospheric pressure, wind speed and direction, and precipitation, were analyzed for the period 2015–2024. Spatial distributions and seasonal variations were visualized using Python programming language, and descriptive statistics were used to identify trends and relationships among parameters.

To ensure consistency, reliability, and comparability across datasets, a systematic methodological framework was implemented. All datasets were standardized to monthly values to enable direct comparison. Missing values in the ERA5 gridded datasets were filled using bilinear interpolation, whereas missing station data were treated with linear temporal interpolation. Quality control involved outlier detection at a ±3 standard deviation threshold, cross-validation between reanalysis and station data, and consistency checks against climatological baselines and supporting references.

EOF analysis was applied to extract the dominant modes of variability in the weather parameters, and correlation and regression analyses were conducted to quantify the strength and nature of the relationships among variables. Mapping tools were used to map the study area and visualize spatial variability. Beyond statistical evaluation, this study also considered the implications of weather changes for local livelihoods and highlighted opportunities for renewable energy, particularly wind power. Input from stakeholders was incorporated to ensure that findings are relevant to community needs and regional planning. Producing accurate weather maps for this coastal belt is especially important in a setting frequently exposed to tropical cyclones and heavy monsoons.

2.3. EOF analysis

The EOF method was used to determine the interdependency and variations of air temperature, atmospheric pressure, humidity, wind speed and direction, and precipitation data. $\sum_{i=1}^{N} \boldsymbol{PC}(t_i)$ was used to deconstruct a variable's time series, where $\sum$ indicates the sum of all terms, i = 1 to N, N is the total number of time steps or observations, and PC (ti) is the principal component value at time ti, representing the temporal variability of the corresponding EOF mode at each iteration [8, 12].

AQ1

2.4. Correlation and regression analysis

Correlation and regression were employed to understand how changes in meteorological parameters are related to other atmospheric variables with a certain lead [13, 14].

$$\mathbf{r}(\tau) = \frac{\sum_{t=1}^{N-|\tau|}(\mathbf{X(t)}-\mathbf{X})\left(\mathbf{Y(t}+\tau)-\overline{\mathbf{Y}}_{\tau}\right)}{\sqrt{\sum_{t=1}^{N-|\tau|}(\mathbf{X(t)}-\mathbf{X})^2 \sum_{t=1}^{N-|\tau|}\left(\mathbf{Y(t}+\tau)-\overline{\mathbf{Y}}_{\tau}\right)^2}}$$

where τ is the lag in time units (positive if Y lags behind X), N is the length of the overlapping time series after accounting for the lag, and $\bar{X}$ and $\bar{Y}\tau$ are the means of X and the lagged Y, respectively.

3. Results

3.1. Air temperature

3.1.1. Spatial distribution of yearly air temperature

Figure 2 presents contour maps of annual air temperature across the Cox's Bazar–Teknaf region from 2015 to 2024. In 2015, average temperatures are approximately 22.5°C, shown by the prevalence of cooler tones. In 2017, a gradual warming becomes visible, with shades shifting slightly and the mean temperature increasing to approximately 23.0°C. The signal strengthens in 2020 as yellow and orange hues appear, indicating an average of approximately 23.5°C. This upward trend peaks in 2024, when widespread warmer shades reflect an average near 24.0°C. The contour lines, which connect areas of equal temperature, further highlight the steady spatial expansion of warmth across the region. Overall, the maps reveal a clear annual warming trend with significant implications for regional temperature change.

3.1.2. Yearly mean of air temperature from secondary data sources and BMD data for validation

Table 1 displays the values comparing the yearly mean air temperatures from 2015 to 2024 based on two data sources: secondary data and data from the BMD. According to the secondary data, the mean temperature starts at approximately 26.03°C in 2015, fluctuates slightly over the years, reaching a peak of 26.56°C in 2023, and ends at 26.81°C in 2024. Conversely, the BMD data show a more consistent upward trend, starting at 26.0°C in 2015, gradually increasing to 26.7°C in 2023, and slightly decreasing to 26.5°C in 2024, with a minor dip to 26.1°C in 2020. Both datasets indicate a general warming trend over the decade, with the BMD data reflecting consistently higher temperatures compared to the secondary data for most of the period. This comparison highlights the variations that can exist between different data sources when analyzing climate trends in the region.

3.1.3. Trend analysis of air temperature

Figure 3 presents two-line graphs depicting monthly or seasonal air temperature trends from 2015 to 2024, sourced from secondary data (top graph) and the BMD data (bottom graph). In the secondary data, the temperatures exhibit significant intra-annual fluctuations, ranging from lows reaching approximately 21°C–22°C to highs reaching approximately 29°C–30°C in various years. Although it is challenging to pinpoint a single "average" starting point due to these fluctuations, the overall trend shows prominent seasonal cycles with peaks generally occurring around the middle of each year. The BMD data also reflect intra-annual variability, with temperatures fluctuating between approximately 21°C and 23°C at their lowest and reaching peaks of approximately 28°C–29°C. Similar to the secondary data, a clear seasonal pattern is evident. As shown in both graphs, although there are differences in the magnitude of the fluctuations and the peak temperatures recorded by each source, both datasets illustrate recurring seasonal temperature variations throughout the 2015–2024 period. Analyzing long-term trends would require examining the overall pattern and potentially calculating yearly averages from this higher-resolution data.

3.1.4. Spatial distribution of monthly air temperature

Figure 4 shows the monthly averaged variation air temperature across the Cox's Bazar–Teknaf region using data from 2015 to 2024. In January, temperatures range from approximately 20°C to 22°C and increase steadily to 25°C–27°C by April. The highest values appear in May and June, averaging approximately 28°C and occasionally

[3] BMD data portal: https://dataportal.bmd.gov.bd

Figure 2
Yearly spatiotemporal distribution of air temperature (°C) in the Cox's Bazar–Teknaf region from 2015 to 2024

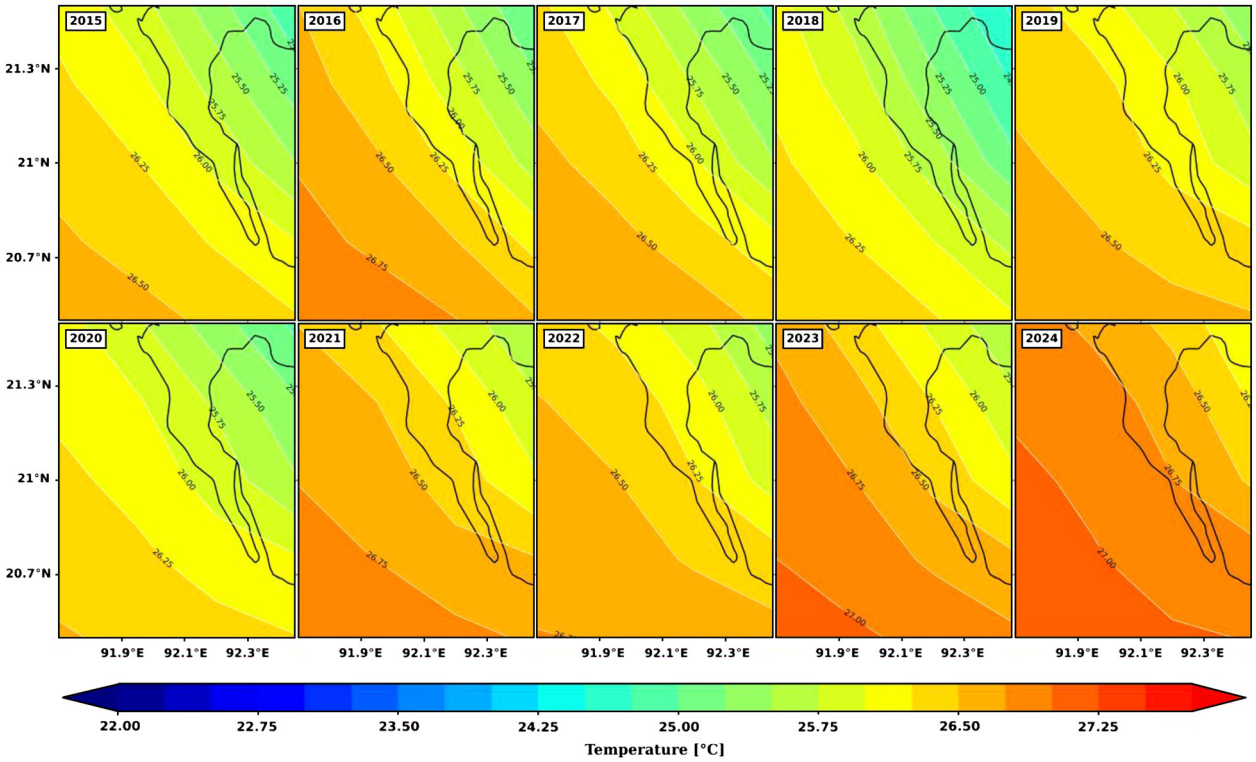

exceeding 29°C in some areas. Temperatures then decrease gradually, with July and August averaging 27°C–28°C. This cooling trend continues through the later months, with November ranging between 24°C and 26°C and December decreasing slightly to 23°C–25°C.

3.1.5. Monthly mean of air temperature

Table 2 displays the values illustrating the monthly mean air temperatures from January to December for the years 2015–2024 based on secondary data and data from the BMD. According to the secondary data, the monthly mean temperature starts at approximately 21.39°C in January, increases to a peak of 28.91°C in May, and then gradually decreases to 23.05°C in December. There is a secondary peak in April at 28.32°C and a slight dip in June to 27.83°C. In contrast, the BMD data show a similar seasonal pattern but with generally lower temperatures in the initial and final months. It begins at 20.8°C in January, increases to a peak of 29.4°C in May, and decreases to 22.4°C in December. Similar to the secondary data, there is a notable increase in April to 28.7°C and a slight decrease in June to 28.2°C. Both datasets clearly illustrate the seasonal temperature fluctuations in the region, with the highest temperatures occurring around April–May and the lowest in January and December. Although there are some differences in the magnitude of the recorded temperatures between the two sources, the overall trend of seasonal variation is consistent, underscoring the importance of monitoring these patterns for effective environmental management.

3.1.6. Seasonal climatology of air temperature

Figure 5 presents the seasonal variation in air temperature across the Cox's Bazar–Teknaf region between 2015 and 2024, grouped into winter, spring, summer, and autumn. Winter shows the lowest values, generally between 21°C and 23.5°C, illustrated in cooler shades of blue

Figure 3
Time series analysis of air temperature (°C) from 2015 to 2024. (a) Secondary data and (b) BMD data illustrate decadal fluctuations over time

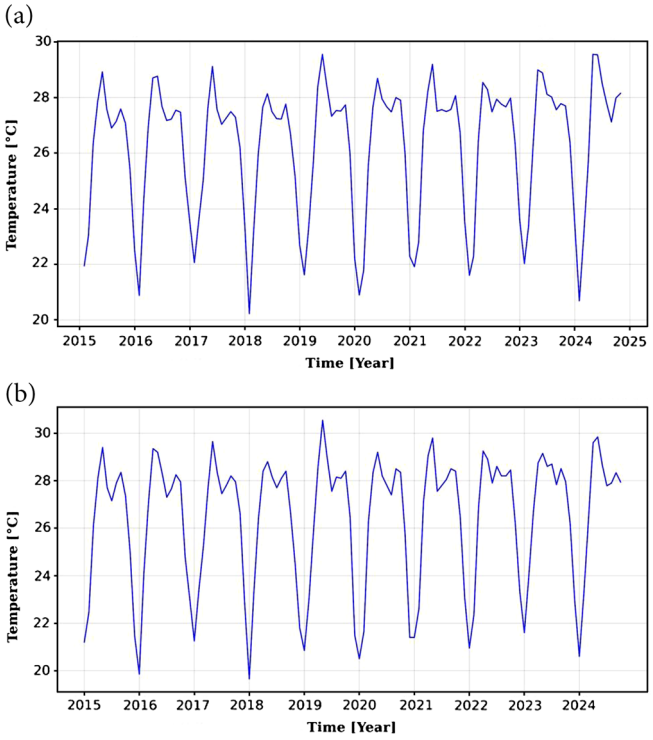

Table 1
Yearly average air temperature (°C) values from 2015 to 2024 based on both secondary sources and BMD data

Yearly mean air temperature (°C) of 2015–2024										
Data sources	**2015**	**2016**	**2017**	**2018**	**2019**	**2020**	**2021**	**2022**	**2023**	**2024**
Secondary data	26.03	26.28	26.14	25.79	26.26	25.99	26.45	26.33	26.56	26.81
BMD data	26.0	26.4	26.4	26.0	26.5	26.1	26.6	26.6	26.7	26.5

Figure 4
Monthly spatiotemporal distribution of air temperature (°C) in the Cox's Bazar–Teknaf region from 2015 to 2024

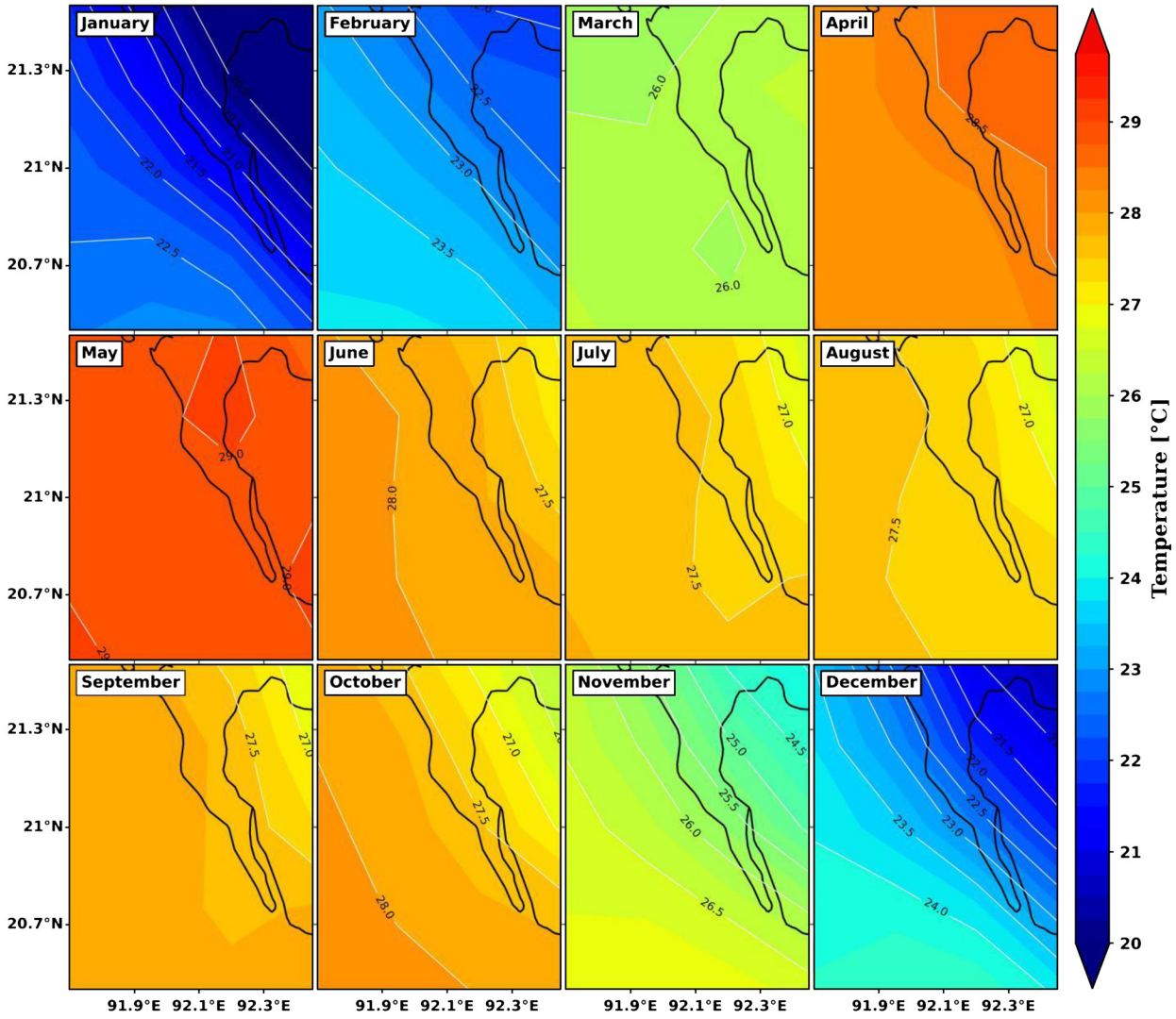

Table 2
Monthly average air temperature (°C) values from 2015 to 2024 based on both secondary sources and BMD data

Monthly mean air temperature (°C) of 2015–2024												
Data sources	**Jan**	**Feb**	**Mar**	**Apr**	**May**	**Jun**	**Jul**	**Aug**	**Sept**	**Oct**	**Nov**	**Dec**
Secondary data	21.39	23.05	26.08	28.32	28.91	27.83	27.47	27.38	27.69	27.61	25.95	23.05
BMD data	20.8	23.0	26.4	28.7	29.4	28.2	27.8	27.9	28.3	27.9	25.8	22.4

and green. Temperatures increase in spring, reaching approximately 27°C–28°C, marked by warmer tones of orange and red. Summer records the peak values, often exceeding 27°C, and autumn reflects a modest decrease to approximately 26°C–27.5°C.

3.1.7. Seasonal mean of air temperature

Table 3 summarizes the average seasonal air temperatures in the Cox's Bazar–Teknaf region between 2015 and 2024 using both secondary and BMD datasets. The secondary data indicate mean values

Figure 5
Seasonal spatiotemporal distribution of air temperature (°C) in the Cox's Bazar–Teknaf region from 2015 to 2024

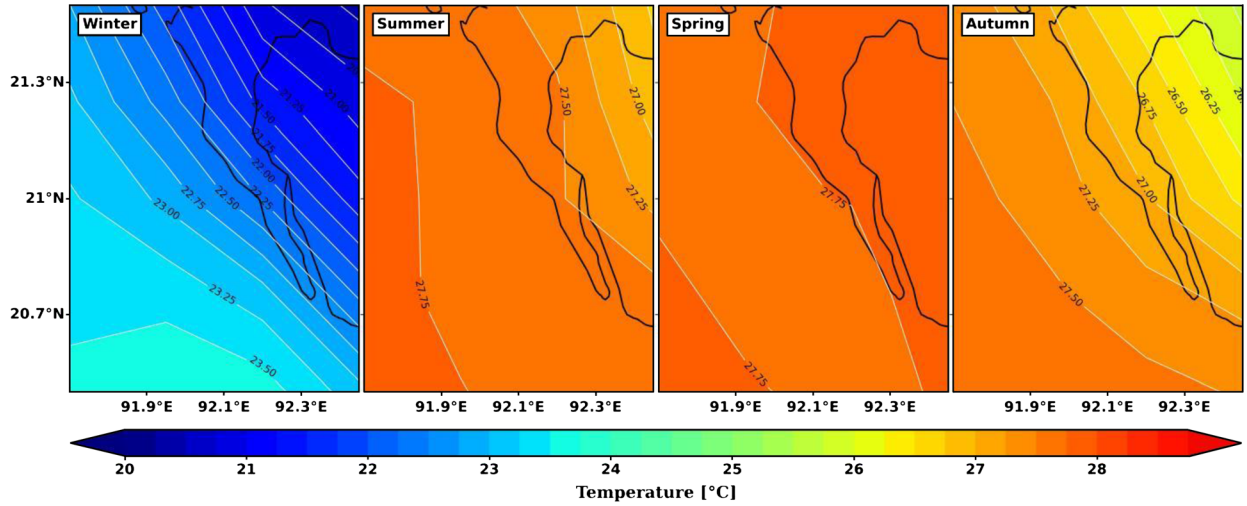

Table 3
Seasonal average air temperature (°C) values from 2015 to 2024 based on both secondary sources and BMD data

Seasonal mean air temperature (°C) of 2015–2024				
Data sources	**Winter**	**Summer**	**Spring**	**Autumn**
Secondary data	22.48	27.56	27.77	27.12
BMD data	22.1	28.0	28.2	27.3

of approximately 22.5°C in winter, 27.8°C in spring, 27.6°C in summer, and 27.1°C in autumn. The BMD records show a comparable pattern, with averages of 22.1°C in winter, 28.2°C in spring, 28.0°C in summer, and 27.3°C in autumn. In both datasets, spring emerges as the warmest season, closely followed by summer.

3.2. Atmospheric pressure

3.2.1. Spatial distribution of yearly surface pressure

Figure 6 depicts annual variations in surface pressure across the Cox's Bazar–Teknaf region from 2015 to 2024. Between 2015 and

Figure 6
Yearly spatiotemporal distribution of surface pressure (mbar) in the Cox's Bazar–Teknaf region from 2015 to 2024

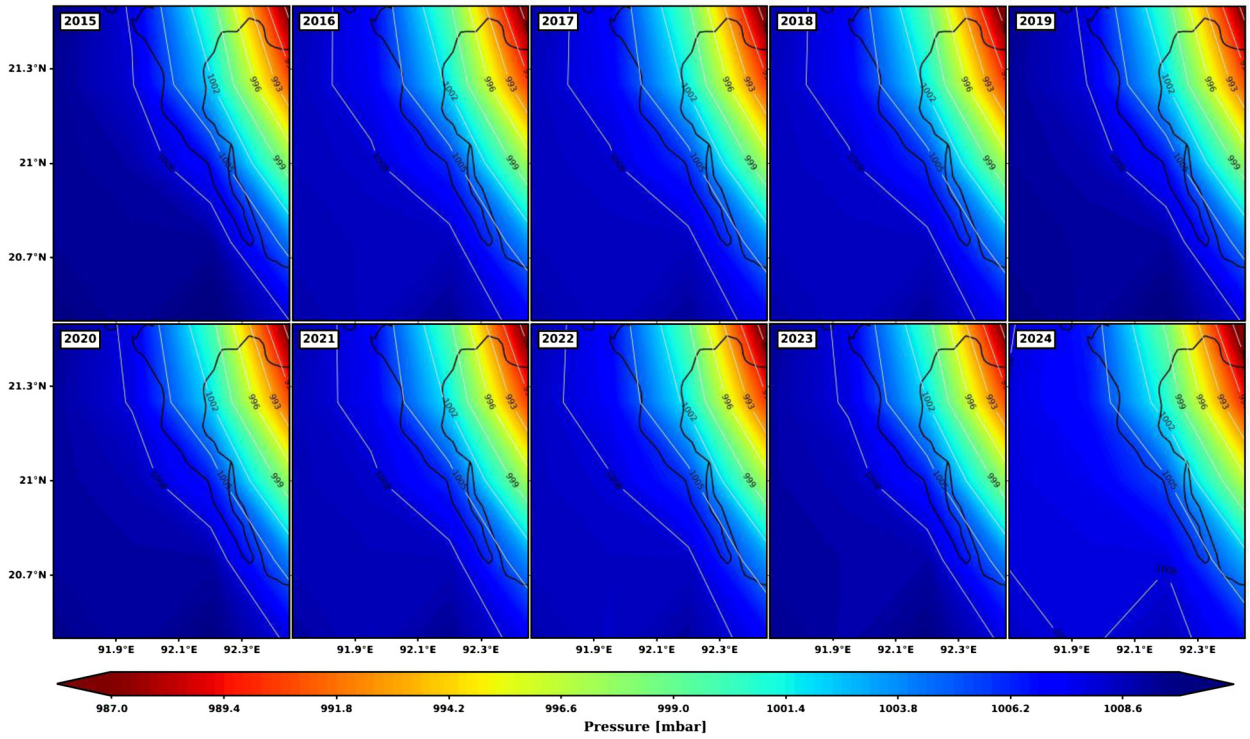

2017, the region experienced relatively high pressures (approximately 1002–1004 mbar), shown in shades of blue. Pressures decreased slightly in 2018 and 2019 (approximately 1001–1002 mbar), reflected by greens and yellows. By 2020, further decreases to approximately 999–1001 mbar are indicated by warmer shades of yellow and orange. Subsequent years showed variable patterns: 2021 and 2023 resembled 2019 levels, and 2022 recorded slightly lower pressures (1000–1002 mbar). In 2024, cooler tones returned, suggesting an increase to 1002–1003 mbar.

3.2.2. Yearly mean of surface pressure

Table 4 shows the average values of yearly surface pressure in the Cox's Bazar–Teknaf region from 2015 to 2024. The top portion relies on secondary data, and the bottom one presents information from the BMD. The secondary data show yearly mean surface pressure starting at approximately 1005.3 mbar in 2015, with minor ups and downs, peaking at 1005.2 mbar in 2019, and finishing at 1003.9 mbar in 2024. The BMD data follow a similar pattern, beginning at 1009.1 mbar in 2015, peaking at 1008.9 mbar in 2019, and ending at 1008.9 mbar in 2024. Both charts consistently show that the yearly average surface pressure remained fairly stable over the decade. Interestingly, the BMD data consistently recorded slightly higher-pressure values than the secondary data. These charts effectively highlight the subtle year-to-year shifts in surface pressure within the region.

3.2.3. Trend analysis of surface pressure

Figure 7 shows two-line graphs depicting surface pressure trends in the Cox's Bazar–Teknaf region from 2015 to 2024 based on secondary data (top) and BMD data (bottom). In the secondary dataset, surface pressure exhibits distinct seasonal fluctuations, ranging from approximately 998 to 1012 mbar. It starts near 1000–1001 mbar in early 2015 and follows a consistent pattern of annual increases and decreases, with notable dips around 2019 and 2020. Despite these variations, the overall trend remains relatively stable. The BMD data display a similar cyclical pattern, varying between approximately 1000 mbar and peaks of 1016–1018 mbar, beginning around 1012–1013 mbar in 2015 and showing a pronounced decrease around 2020. Together, these graphs illustrate the dynamic nature of surface pressure in the region.

3.2.4. Monthly climatology of surface pressure

Figure 8 presents contour maps of the average monthly surface pressure across the Cox's Bazar–Teknaf region using data from 2015 to 2024.

In January, the region experiences high pressures ranging from approximately 1006 to 1012 mbar, shown in shades of blue. Pressures decrease slightly in February, falling between 1003 and 1009 mbar, with green tones becoming more prominent. The downward trend continues through March (1000–1006 mbar) and April (997–1003 mbar), indicated by green and yellow hues. May records the lowest pressures of the year, decreasing below 991 mbar in some areas, represented by dominant red and orange shades. Pressure begins to increase in June (994–1000 mbar) and continues through July and August (997–1003 mbar). In September, pressures average 1000–1006 mbar, increasing further in October (1003–1009 mbar), November (1006–1012 mbar), and December, which resembles January's pattern.

Figure 7
Time series analysis of surface pressure (mbar) from 2015 to 2024. (a) Secondary data and (b) BMD data illustrate decadal fluctuations over time

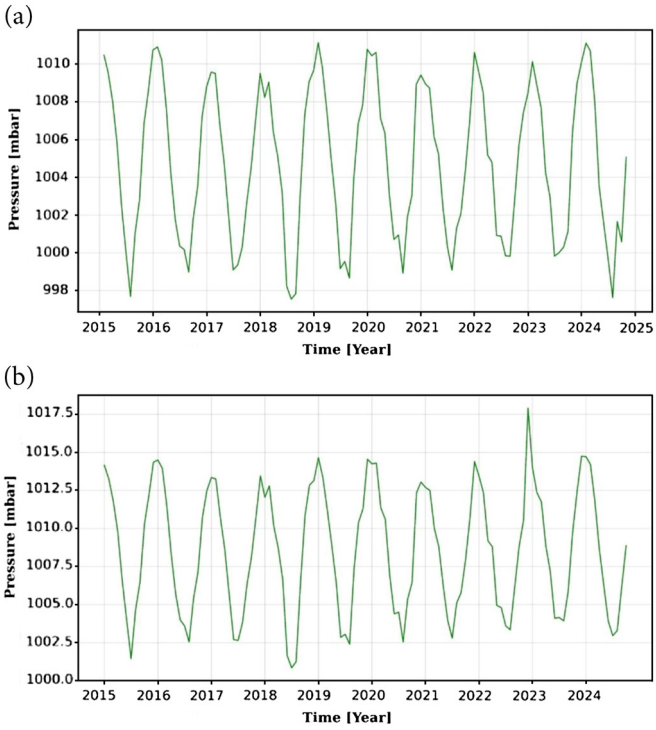

3.2.5. Monthly mean of surface pressure

Table 5 shows the monthly mean surface pressure values from 2015 to 2024 for the Cox's Bazar–Teknaf region based on secondary data and data from the BMD. In the secondary data, the monthly mean surface pressure starts at approximately 1010.0 mbar in January and decreases to 1009.6 mbar in February and 1007.0 mbar in March. Pressure then increases to 1004.9 mbar in April and 1002.3 mbar in May, reaching a low of 999.8 mbar in June and July. It then slightly increases to 999.9 mbar in August and 1002.2 mbar in September, increasing further to 1003.4 mbar in October and 1006.0 mbar in November before peaking at 1009.8 mbar in December. In the BMD data, the monthly mean surface pressure begins at 1013.8 mbar in January and decreases to 1011.2 mbar in February and 1010.9 mbar in March. It then decreases further to 1009.0 mbar in April and 1006.2 mbar in May, reaching a low of 1003.6 mbar in June and 1003.0 mbar in July. It then increases to 1003.3 mbar in August and 1006.1 mbar in September, increasing to 1008.9 mbar in October and 1011.5 mbar in November before peaking at 1014.2 mbar in December.

3.2.6. Spatial distribution of seasonal surface pressure

Figure 9 presents contour maps showing seasonal variations in surface pressure across the Cox's Bazar–Teknaf region from 2015

Table 4
Yearly average surface pressure (mbar) values from 2015 to 2024 based on both secondary sources and BMD data

	Yearly mean surface pressure (mbar) of 2015–2024									
Data sources	**2015**	**2016**	**2017**	**2018**	**2019**	**2020**	**2021**	**2022**	**2023**	**2024**
Secondary data	1005.3	1004.6	1004.6	1004.6	1005.2	1005.1	1004.7	1004.5	1005.1	1003.9
BMD data	1009.1	1008.3	1008.3	1008.1	1008.9	1008.8	1008.4	1008.7	1009.1	1008.9

Figure 8
Monthly spatiotemporal distribution of surface pressure (mbar) in the Cox's Bazar–Teknaf region from 2015 to 2024

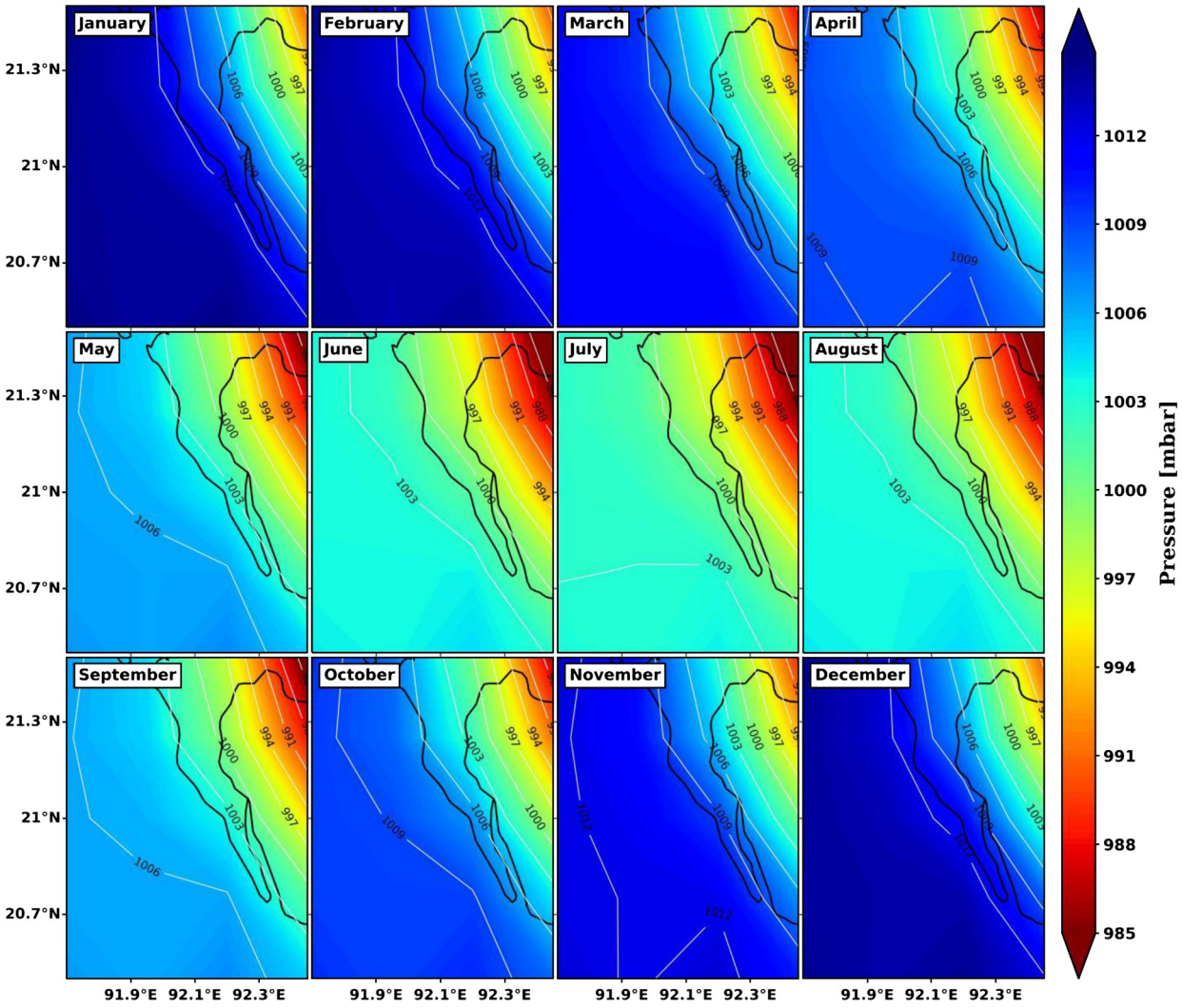

Table 5
Monthly average surface pressure (mbar) values from 2015 to 2024 based on both secondary sources and BMD data

Monthly mean surface pressure (mbar) of 2015–2024												
Data sources	**Jan**	**Feb**	**Mar**	**Apr**	**May**	**Jun**	**Jul**	**Aug**	**Sept**	**Oct**	**Nov**	**Dec**
Secondary data	1010.0	1009.6	1007.0	1004.9	1002.3	999.8	999.2	999.9	1002.2	1005.4	1008.0	1009.8
BMD data	1013.8	1013.2	1010.9	1009.0	1006.2	1003.6	1003.0	1003.3	1006.1	1008.9	1011.5	1014.2

to 2024, divided into winter, spring, summer, and autumn. In winter, surface pressure is generally high, ranging from approximately 1006 to over 1013 mbar, depicted in blue and light blue shades. During spring, pressures decrease, with most areas between 997 and 1006 mbar, highlighted in green and yellow. Summer shows the lowest pressures, with large parts of the region below 991 mbar and up to approximately 997 mbar, indicated by red and orange tones, likely reflecting warmer temperatures. In autumn, pressure increases slightly compared to that in summer, typically ranging from 994 to 1003 mbar, shown in yellow and green shades. These seasonal patterns reveal the dynamic nature of atmospheric pressure in the region.

3.2.7. Seasonal mean of surface pressure

Table 6 represents the seasonal mean surface pressure values from 2015 to 2024 of the Cox's Bazar–Teknaf region based on secondary data and data from the BMD. In the secondary data, the average surface pressure is approximately 1009.8 mbar in winter, decreasing slightly to 1004.7 mbar in spring and further to 999.6 mbar in summer. Autumn shows a recovery to 1005.1 mbar. The BMD data show a similar seasonal pattern but with generally higher-pressure values. Winter averages approximately 1013.7 mbar, decreasing to 1008.7 mbar in spring and further to 1003.3 mbar in summer. Autumn shows a recovery to 1008.8 mbar. Both datasets illustrate a consistent seasonal pattern

Figure 9
Seasonal spatiotemporal distribution of surface pressure (mbar) in the Cox's Bazar–Teknaf region from 2015 to 2024

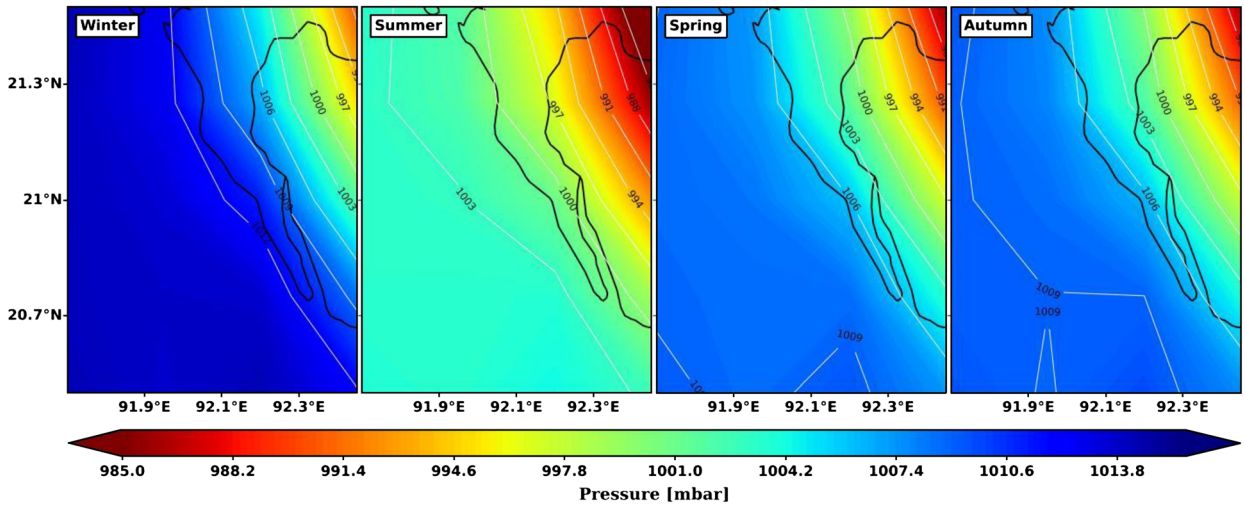

Table 6
Seasonal average surface pressure (mbar) values from 2015 to 2024 based on both secondary sources and BMD data

Seasonal mean surface pressure (mbar) of 2015–2024				
Data sources	**Winter**	**Summer**	**Spring**	**Autumn**
Secondary data	1009.8	999.6	1004.7	1005.1
BMD data	1013.7	1003.3	1008.7	1008.8

with higher mean surface pressure during winter and autumn and lower mean surface pressure during spring and summer.

3.3. Humidity

3.3.1. Spatial variation of yearly relative humidity

Figure 10 presents contour maps illustrating annual variations in relative humidity across the Cox's Bazar–Teknaf region from 2015 to 2024. In 2015, relative humidity was moderate, ranging mostly between

Figure 10
Yearly spatiotemporal distribution of relative humidity (%) in the Cox's Bazar–Teknaf region from 2015 to 2024

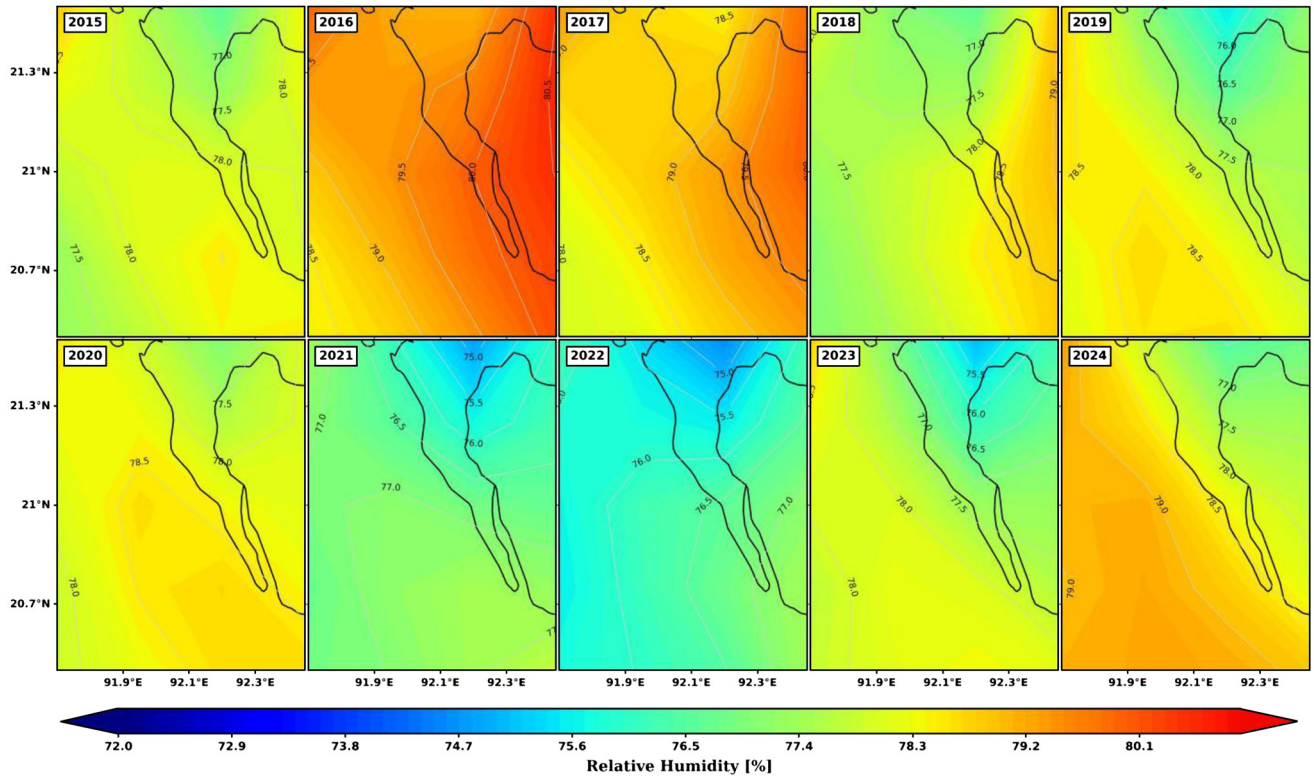

74% and 76%. It increased slightly in 2016, with more areas at 76%–78%, and peaked in 2017, when large parts of the region reached 78%–80% or higher. Humidity decreased slightly in 2018 (75%–77%) and 2019 (74%–76%), increased again in 2020 (76%–78%), and showed a minor decrease in 2021, similar to that in 2019. A notable increase occurred in 2022, reaching approximately 78%–80%, followed by a slight decrease in 2023 (76%–78%). In 2024, humidity displayed a mixed pattern, generally ranging from 75% to 77%. These annual fluctuations highlight the variability of the region's decadal climate.

3.3.2. Yearly mean of relative humidity

Table 7 presents the yearly mean relative humidity values from 2015 to 2024 for the Cox's Bazar–Teknaf region based on secondary data and data from the BMD. In the secondary data, the yearly mean relative humidity starts at approximately 77.95% in 2015, increases to 79.54% in 2016, and peaks at 78.95% in 2017. It then decreases to 77.92% in 2018 and 77.87% in 2019. In 2020, humidity increases to 78.21%, followed by a slight decrease to 76.76% in 2021 and further to 76.18% in 2022. The trend then increases to 77.55% in 2023 and 78.45% in 2024. The BMD data show a generally higher mean relative humidity across the years, starting at approximately 79.96% in 2015, increasing to 80.21% in 2016, and then decreasing to 79.29% in 2017 and 79.0% in 2018. It further decreases to 77.08% in 2019 and then increases to 77.42% in 2020 and 78.67% in 2021, peaking at 77.83% in 2022 before decreasing to 77.65% in 2023 and increasing slightly to 77.81% in 2024. Both datasets illustrate relatively high yearly mean relative humidity in the region with some interannual variability.

3.3.3. Trend analysis of relative humidity

Figure 11 presents two-line graphs showing relative humidity trends in the Cox's Bazar–Teknaf region from 2015 to 2024 based on secondary data (top) and BMD data (bottom). In the secondary dataset, humidity fluctuates throughout each year, ranging from approximately 62%–65% at the lowest to 88%–90% at the highest. The graph reveals a recurring seasonal cycle, with peaks typically in the middle and end of the year, particularly around mid-2017 and late 2022, and the lowest values occur in the early months. The BMD data display a similar pattern, with values ranging from approximately 66%–70% and highs of 90%–92%, following the same annual pattern.

3.3.4. Monthly climatology of relative humidity

Figure 12 shows a series of contour maps illustrating the average monthly relative humidity in the Cox's Bazar–Teknaf region, likely based on data from 2015 to 2024 and organized by month. Each map uses a color gradient to represent humidity percentages, with warmer colors such as yellow, orange, and red indicating higher humidity and cooler tones such as green and blue showing lower levels. In January, humidity is relatively low, ranging from approximately 63% to 72%. February sees a slight increase, with values between 66% and 75%. March brings a more noticeable increase, with humidity ranging from 70% to 78%. April continues this upward trend, reaching between 75% and 82%. May records the highest humidity levels of the year, with much of the region showing values above 82% and reaching over 89%. June remains very humid, with levels between 79% and 86%, followed by similarly high humidity in July and August. In September, humidity starts to decrease slightly, generally falling between 75% and 82%. October shows a small rebound to approximately 78%–86%. November marks a more significant decrease to approximately 72%–80%, and December records the lowest humidity levels of the year, ranging from 60% to 70%. These monthly variations clearly reflect the seasonal nature of the region's humid climate, with peak moisture during the summer months from May to August and drier conditions in the winter from December to February.

Figure 11
Time series analysis of relative humidity (%) from 2015 to 2024. (a) Secondary data and (b) BMD data illustrate decadal fluctuations over time

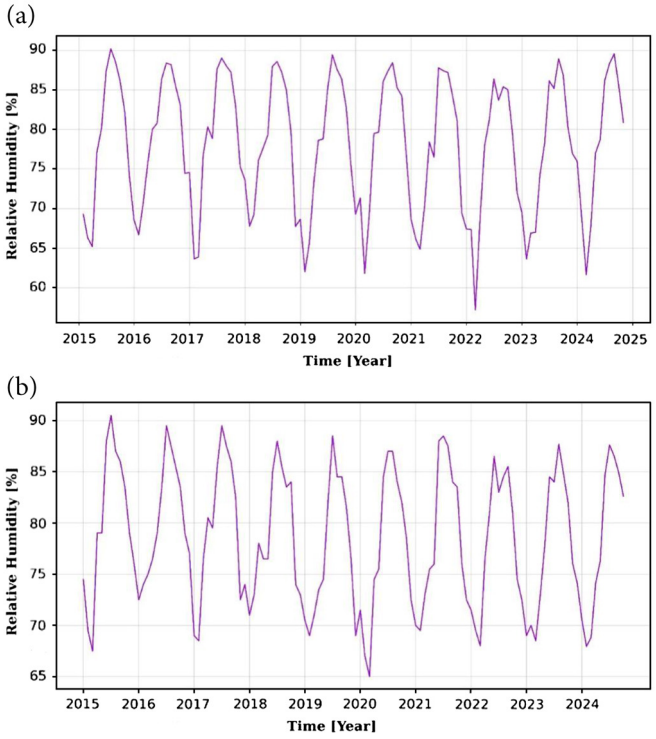

3.3.5. Monthly mean of relative humidity

Table 8 displays the monthly mean relative humidity values from 2015 to 2024 for the Cox's Bazar–Teknaf region based on secondary data and data from the BMD. In the secondary data, the monthly mean relative humidity starts at approximately 66.65% in January, decreases to 64.8% in February, and then increases to 71.09% in March, 78.09% in April, 79.23% in May, and 86.72% in June, peaking at 87.78% in July and remaining high at 87.93% in August. It then decreases to 85.75% in September, 81.66% in October, and 73.59% in November and reaches its lowest at 70.71% in December. The BMD data show a similar seasonal pattern with generally higher humidity in the middle of the

Table 7
Yearly average relative humidity (%) values from 2015 to 2024 based on both secondary sources and BMD data

	Yearly mean relative humidity (%) of 2015–2024									
Data sources	**2015**	**2016**	**2017**	**2018**	**2019**	**2020**	**2021**	**2022**	**2023**	**2024**
Secondary data	77.95	79.54	78.95	77.92	77.87	78.21	76.76	76.18	77.55	78.45
BMD data	79.96	80.21	79.29	79.0	77.08	77.42	78.67	77.83	77.65	77.81

Figure 12
Monthly spatiotemporal distribution of relative humidity (%) in the Cox's Bazar–Teknaf region from 2015 to 2024

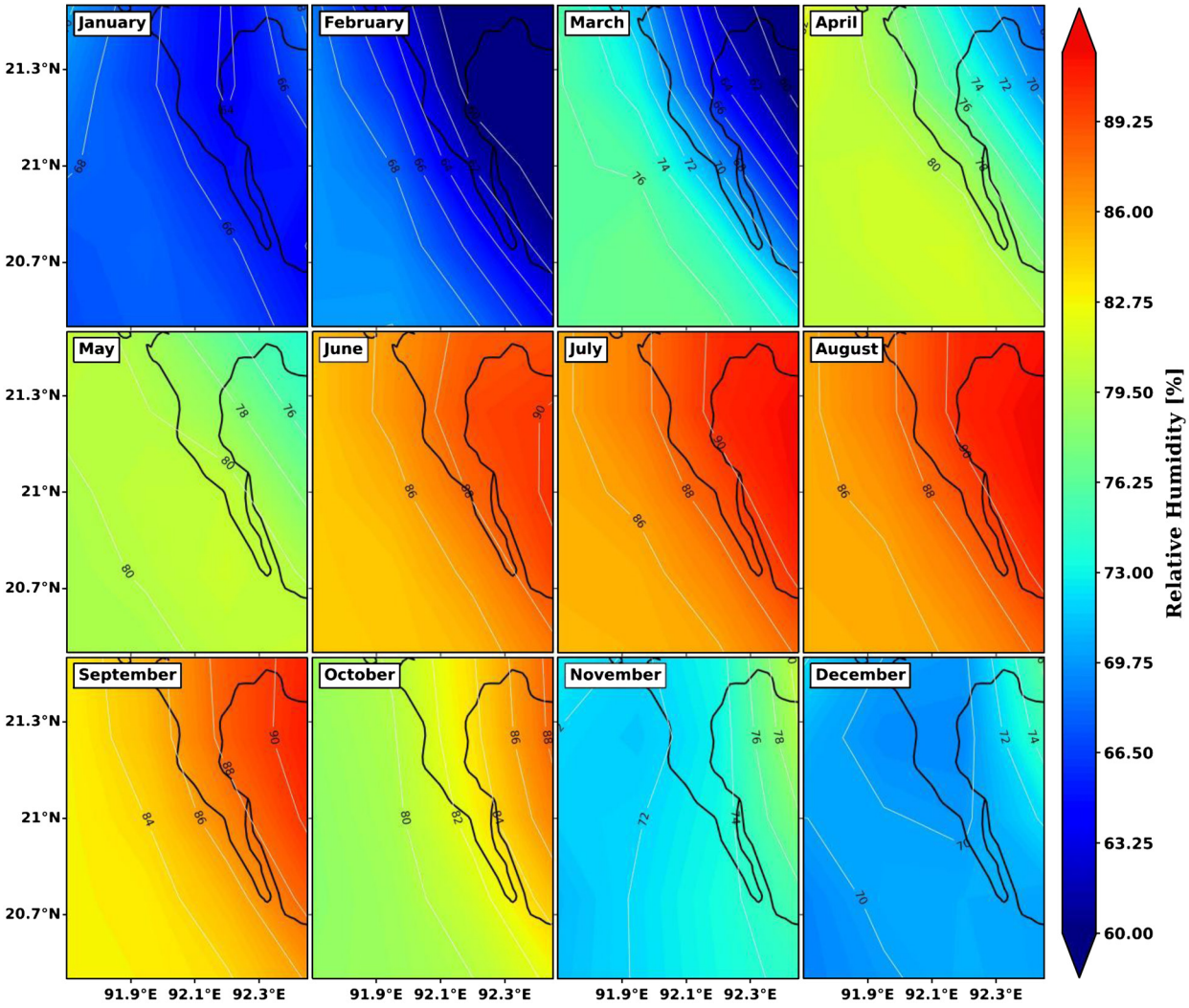

Table 8
Monthly average relative humidity (%) values from 2015 to 2024 based on both secondary sources and BMD data

	Monthly mean relative humidity (%) of 2015–2024											
Data sources	**Jan**	**Feb**	**Mar**	**Apr**	**May**	**Jun**	**Jul**	**Aug**	**Sept**	**Oct**	**Nov**	**Dec**
Secondary data	66.65	64.8	71.09	78.09	79.23	86.72	87.78	87.93	85.75	81.66	73.59	70.71
BMD data	71.01	69.79	71.13	75.97	77.53	85.22	87.61	86.52	84.88	82.61	76.23	73.4

year. It begins at 71.01% in January, decreases to 69.79% in February, and then increases to 71.13% in March, 75.97% in April, 77.53% in May, and 85.22% in June, peaking at 87.61% in July and remaining high at 86.52% in August. It then decreases to 84.88% in September, 82.61% in October, and 76.23% in November and reaches its lowest at 73.4% in December. Both datasets illustrate a clear seasonal pattern with higher mean relative humidity during the summer months (June–August) and lower values during the winter months (December–February).

3.3.6. Spatial distribution of seasonal relative humidity

Figure 13 illustrates seasonal variations in relative humidity across the Cox's Bazar–Teknaf region from 2015 to 2024, categorized into winter, spring, summer, and autumn. In winter, humidity is relatively low, ranging from approximately 60% to 70%, depicted in blue and light green shades, indicating drier conditions. During spring, humidity increases to approximately 70%–80%, shown in green and yellow tones. Summer exhibits the highest levels, with large areas reaching 82%–89% or more, highlighted in orange and red, reflecting the region's warm and moist climate. In autumn, humidity decreases slightly from the summer peak, ranging from 75% to 86% and represented by yellow to orange shades. These patterns demonstrate clear seasonal shifts, with drier conditions in winter and maximum moisture during summer.

3.3.7. Seasonal mean of relative humidity

Table 9 presents the seasonal average relative humidity in the Cox's Bazar–Teknaf region from 2015 to 2024 based on secondary data

Figure 13
Seasonal spatiotemporal distribution of relative humidity (%) in the Cox's Bazar–Teknaf region from 2015 to 2024

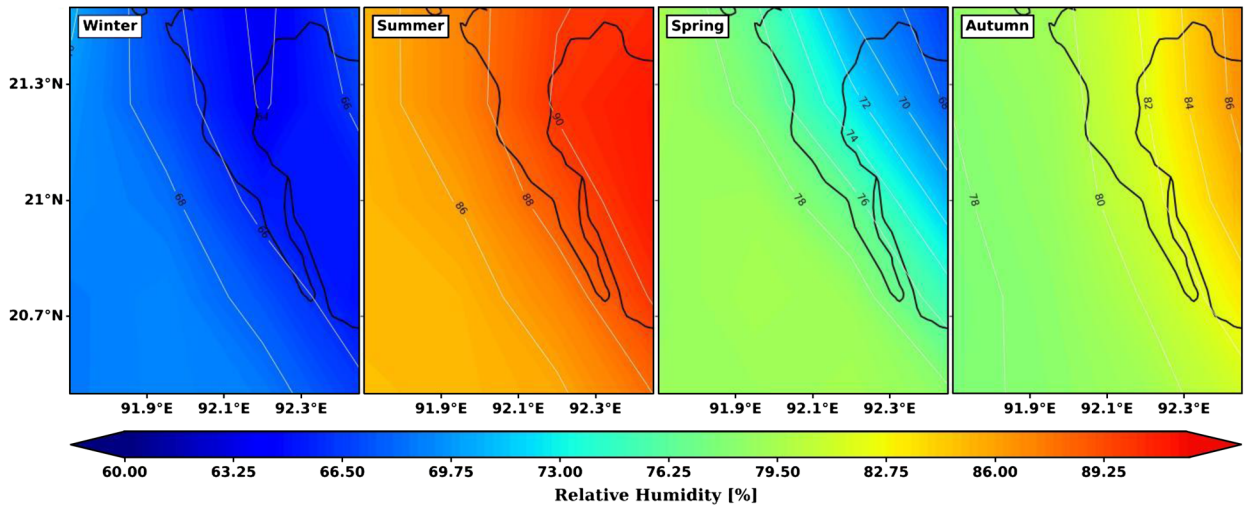

Table 9
Seasonal average relative humidity (%) values from 2015 to 2024 based on both secondary sources and BMD data

Seasonal mean relative humidity (%) of 2015–2024				
Data sources	**Winter**	**Summer**	**Spring**	**Autumn**
Secondary data	67.27	76.14	87.48	80.57
BMD data	71.4	74.88	86.45	81.24

and BMD records. According to the secondary data, humidity is lowest in winter at 67.27%, increases to 76.14% in spring, reaches the highest level in summer at 87.48%, and then slightly decreases to 80.57% in autumn. The BMD data reveal a similar pattern, with winter averaging 71.4%, spring at 74.88%, summer peaking at 86.5%, and autumn at 81.24%.

3.4. Wind speed and direction

3.4.1. Spatial distribution of yearly wind speed and direction

Figure 14 shows annual variations in surface wind speed and direction across the Cox's Bazar–Teknaf region from 2015 to 2024. Wind speed is represented by a color scale from 0.0 to 4.5 m/s, with cooler shades (blue) indicating lower speeds and warmer tones (yellow and red) higher speeds. White dashed lines depict wind streamlines, indicating general wind direction. From 2015 to 2017, wind speeds were relatively low, typically below 2.0 m/s, as shown by dominant blues and light greens, with winds primarily flowing from the south to southwest. Between 2018 and 2021, speeds increased significantly, with widespread yellow and orange areas representing 3.0–4.5 m/s, and the prevailing southwesterly direction remained consistent. From 2022 to 2024, wind speeds moderated slightly, with more green and blue shades, particularly in 2024, indicating a reduction compared to the previous peak years. Overall, the maps highlight a decade-long trend of increasing wind speeds from 2015 to 2020, followed by a slight decrease, and the dominant wind direction remained consistently southerly to southwesterly.

3.4.2. Yearly mean of wind speed

Table 10 shows the yearly average wind speed values from 2015 to 2024 in the Cox's Bazar–Teknaf region using secondary data and BMD data. According to the secondary data, wind speed was 3.03 m/s in 2015, dipped slightly to 2.81 m/s in 2016, and then showed small fluctuations over the years, with minor increases and decreases, reaching its lowest point of 2.77 m/s in 2021 before returning to 3.03 m/s in 2024. In contrast, the BMD data show generally stronger wind speeds, starting at 3.5 m/s in 2015, increasing steadily to a peak of 4.24 m/s in 2017, then showing a mix of increases and decreases, and ending at 3.81 m/s in 2024. Despite differences in exact values, both datasets show noticeable year-to-year changes, with the BMD records consistently reporting higher wind speeds throughout the period.

3.4.3. Trend analysis of wind speed

Figure 15 shows two-line graphs that track monthly or seasonal wind speed changes from 2015 to 2024 in the Cox's Bazar–Teknaf region using secondary data in the top graph and BMD data in the bottom one. The secondary data reveal noticeable ups and downs throughout each year, with wind speeds ranging from approximately 0.5 to 5.0 m/s. Peaks are especially noticeable around 2017 and 2021, and the lowest speeds are scattered across different months and years. The BMD data show a similar pattern but with generally stronger winds, ranging between approximately 2.5 and 6.0 m/s. It also follows a repeating cycle of increases and decreases, with particularly high speeds seen around 2019.

3.4.4. Monthly climatology of wind speed and direction

Figure 16 shows the average monthly surface wind speed and direction across the Cox's Bazar–Teknaf region based on data from 2015 to 2024. From January to March, wind speeds remain relatively low (1.8–3.0 m/s), accompanied by weak and variable directions. A sharp increase occurs in April and May, with speeds often exceeding 3.6 m/s and a steady southwesterly flow. The strongest winds are recorded during the monsoon months (June–August), when large areas reach above 4.2 m/s, marked by persistent southwesterly winds. After the monsoon, speeds gradually decrease from September to December (1.8–3.6 m/s), and wind direction becomes more variable, shifting toward northerly and northeasterly flows.

3.4.5. Monthly mean of wind speed

Table 11 displays the monthly mean wind speed values from 2015 to 2024 for the Cox's Bazar–Teknaf region based on secondary data and data from the BMD. In the secondary data, the monthly mean wind speed starts at 3.7 m/s in January and decreases to 2.9 m/s in

Figure 14
Yearly spatiotemporal distribution of wind speed (m/s) in the Cox's Bazar–Teknaf region from 2015 to 2024. Wind vectors indicate wind direction, providing a comprehensive view of wind patterns over the years

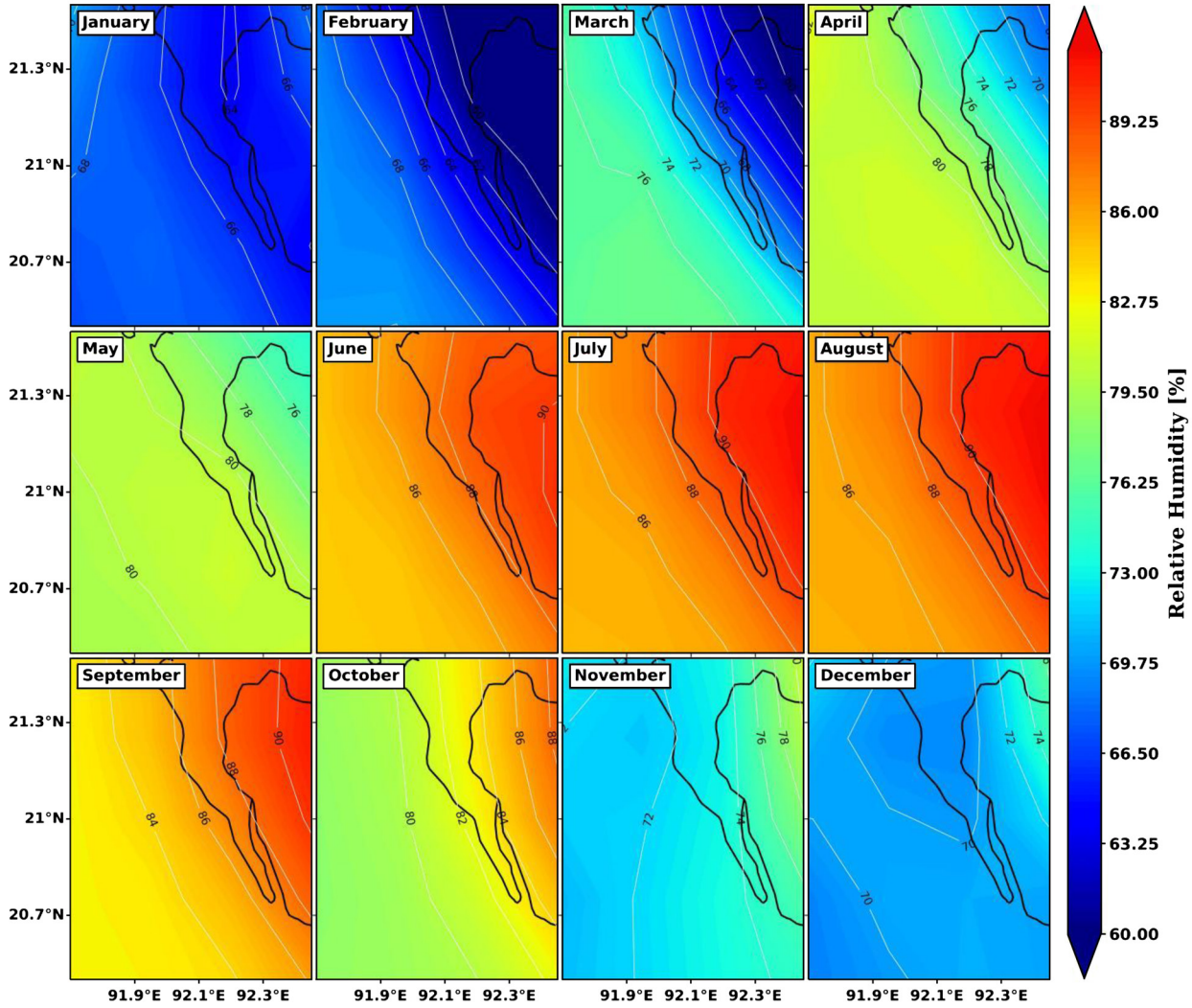

Table 10
Yearly average wind speed (m/s) values from 2015 to 2024 based on both secondary sources and BMD data

Yearly mean wind speed (m/s) of 2015–2024										
Data sources	**2015**	**2016**	**2017**	**2018**	**2019**	**2020**	**2021**	**2022**	**2023**	**2024**
Secondary data	3.03	2.81	2.84	2.93	2.88	3.13	2.77	2.82	2.78	3.03
BMD data	3.5	3.89	4.24	3.69	4.2	3.96	3.4	3.19	3.82	3.81

Table 11
Monthly average wind speed (m/s) values from 2015 to 2024 based on both secondary sources and BMD data

Monthly mean wind speed (m/s) of 2015–2024												
Data sources	**Jan**	**Feb**	**Mar**	**Apr**	**May**	**Jun**	**Jul**	**Aug**	**Sept**	**Oct**	**Nov**	**Dec**
Secondary data	3.7	2.9	2.6	2.4	2.0	3.9	4.5	3.9	2.5	0.8	2.4	3.0
BMD data	3.6	4.2	4.5	3.8	4.0	3.9	3.9	3.9	3.4	3.3	3.3	3.4

Figure 15
Time series analysis of wind speed (m/s) from 2015 to 2024. (a) Secondary data and (b) BMD data illustrate decadal

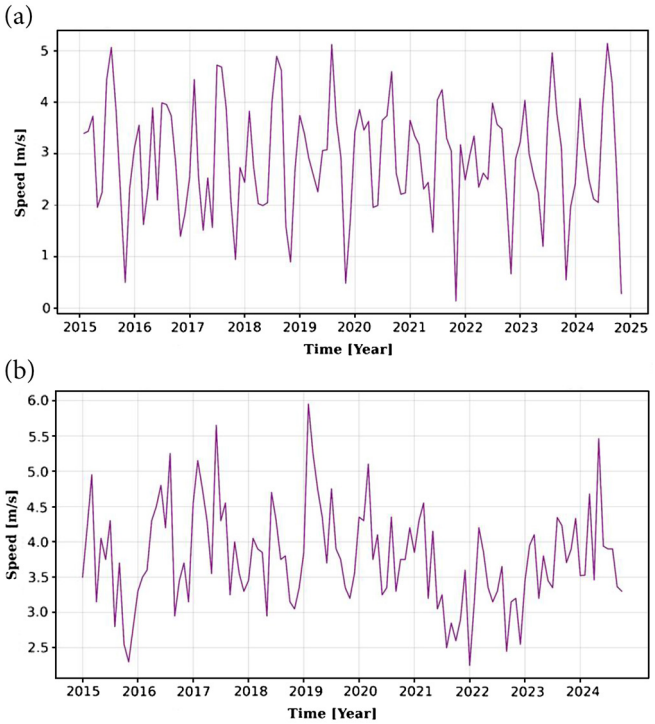

February and 2.6 m/s in March, reaching its lowest point at 2.4 m/s in April and then slightly increasing to 2.0 m/s in May. Wind speed then increases significantly to 3.9 m/s in June and peaks at 4.5 m/s in July and August. It then decreases sharply to 2.5 m/s in September and further to a low of 0.8 m/s in October before increasing to 2.4 m/s in November and 3.0 m/s in December. The BMD data show a different pattern, starting at 3.6 m/s in January, increasing to 4.2 m/s in February, and peaking at 4.5 m/s in March. It then decreases to 3.8 m/s in April and increases again to 4.0 m/s in May, followed by a decrease to 3.9 m/s in June and July, and then slightly decreases to 3.9 m/s in August and 3.4 m/s in September. The wind speed then fluctuates between 3.3 and 3.4 m/s for the remaining months.

3.4.6. Spatial distribution of seasonal wind speed and direction

Figure 17 presents four contour maps that show seasonal patterns of wind speed and direction in the Cox's Bazar–Teknaf region using data from 2015 to 2024. Each map represents a different season: winter, spring, summer, and autumn. Wind speed is shown using a color scale, where blue and green indicate lower speeds and yellow to red represent stronger winds. Black arrows point to the wind direction. In winter, wind speeds usually range from approximately 2.5 to 4.5 m/s, with most areas shaded green to yellow. Spring brings slightly lighter winds, typically between 2.0 and 3.5 m/s, shown in blue and green. Summer experiences the strongest winds of the year, often exceeding 5.5 m/s in many areas, marked by bright yellow, orange, and red. In autumn, wind speeds decrease again, mostly falling between 2.0 and 3.5 m/s, similar to spring.

3.4.7. Seasonal mean of wind speed

Table 12 displays seasonal average wind speed values between 2015 and 2024 in the Cox's Bazar–Teknaf region using secondary data and BMD data. According to the secondary data, wind speeds peak during summer at 4.13 m/s, followed by winter at 3.22, and spring and autumn show lower values at 2.33 and 1.89, respectively. The BMD

Table 12
Seasonal average wind speed (m/s) values from 2015 to 2024 based on both secondary sources and BMD data

Seasonal mean wind speed (m/s) of 2015–2024				
Data sources	**Winter**	**Summer**	**Spring**	**Autumn**
Secondary data	3.22	4.13	2.33	1.89
BMD data	3.7	3.9	4.1	3.3

data also highlight summer as the windiest season at 4.1 m/s but rank the other seasons differently, with autumn at 3.9, winter at 3.7, and spring showing the lowest at 3.3. Despite some variations in the order of seasonal wind speeds, both datasets consistently show clear seasonal changes, highlighting how wind conditions vary throughout the year in this coastal region.

3.5. Precipitation amounts

3.5.1. Spatial distribution of yearly precipitation

Figure 18 show annual rainfall patterns from 2015 to 2024 in the Cox's Bazar–Teknaf region of Bangladesh. Each map illustrates precipitation in millimeters (mm), with blue and green shades indicating lower rainfall and yellow to red shades marking higher amounts, as indicated by the color bar at the bottom.

In 2015, rainfall in the Cox's Bazar–Teknaf region varied from approximately 115 to over 151 mm, with heavier precipitation mostly seen in the eastern areas. The year 2016 brought a general increase in rainfall, with many parts recording over 133 mm. In 2017, high rainfall above 142 mm became more widespread across the region. Although 2018 saw a slight decrease in some locations, it remained fairly wet overall, with most areas receiving more than 124 mm. A noticeable decrease occurred in 2019, with rainfall mostly between 106 and 142 mm. In 2020, precipitation levels picked up again, especially in the central and eastern zones where totals exceeded 142 mm. Rainfall in 2021 was more mixed, with some areas getting over 142 mm and others receiving as little as 115–133 mm. The year 2022 stood out as relatively dry, with most of the region seeing between 97 and 133 mm. Conditions became wetter again in 2023, with large areas receiving more than 142 mm. In 2024, rainfall slightly decreased, generally ranging from 115 to 151 mm. These yearly changes clearly reflect the shifting rainfall patterns across both space and time in this coastal region.

3.5.2. Yearly mean of precipitation

Table 13 shows the yearly precipitation values from 2015 to 2024 based on two different sources: one from secondary data and the other from BMD records. In the secondary data, annual rainfall was 2666.3 mm in 2015 and slightly decreased to 2528.4 mm in 2016. It then peaked at 2678.5 mm in 2017 before decreasing to 2234.0 mm in 2018 and further to 2187.7 mm in 2019. The amount increased again to 2629.5 mm in 2020 but decreased in the following years, reaching 2351.2 mm in 2021 and 1952.9 mm in 2022. In 2023, rainfall increased to 2289.7 mm and reached its highest point in 2024 at 2768.8 mm.

Conversely, the BMD data chart reveals a different pattern. Rainfall in 2015 was exceptionally high at 5081.5 mm and then decreased sharply to 3798.0 mm in 2016. It increased slightly to 4064.5 mm in 2017 before decreasing again to 3781.0 mm in 2018 and 3376.5 mm in 2019. The amount increased to 4000.5 mm in 2020, followed by another decrease to 3263.0 mm in 2021 and a more significant decrease to 2346.0 mm in 2022. In 2023, rainfall slightly increased to 2414.5 mm and increased further to 3467.8 mm in 2024. This comparison highlights not only the differences in the yearly values between the two

Figure 16
Monthly spatiotemporal distribution of wind speed (m/s) in the Cox's Bazar–Teknaf region from 2015 to 2024. Wind vectors indicate wind direction, providing a comprehensive view of monthly wind patterns

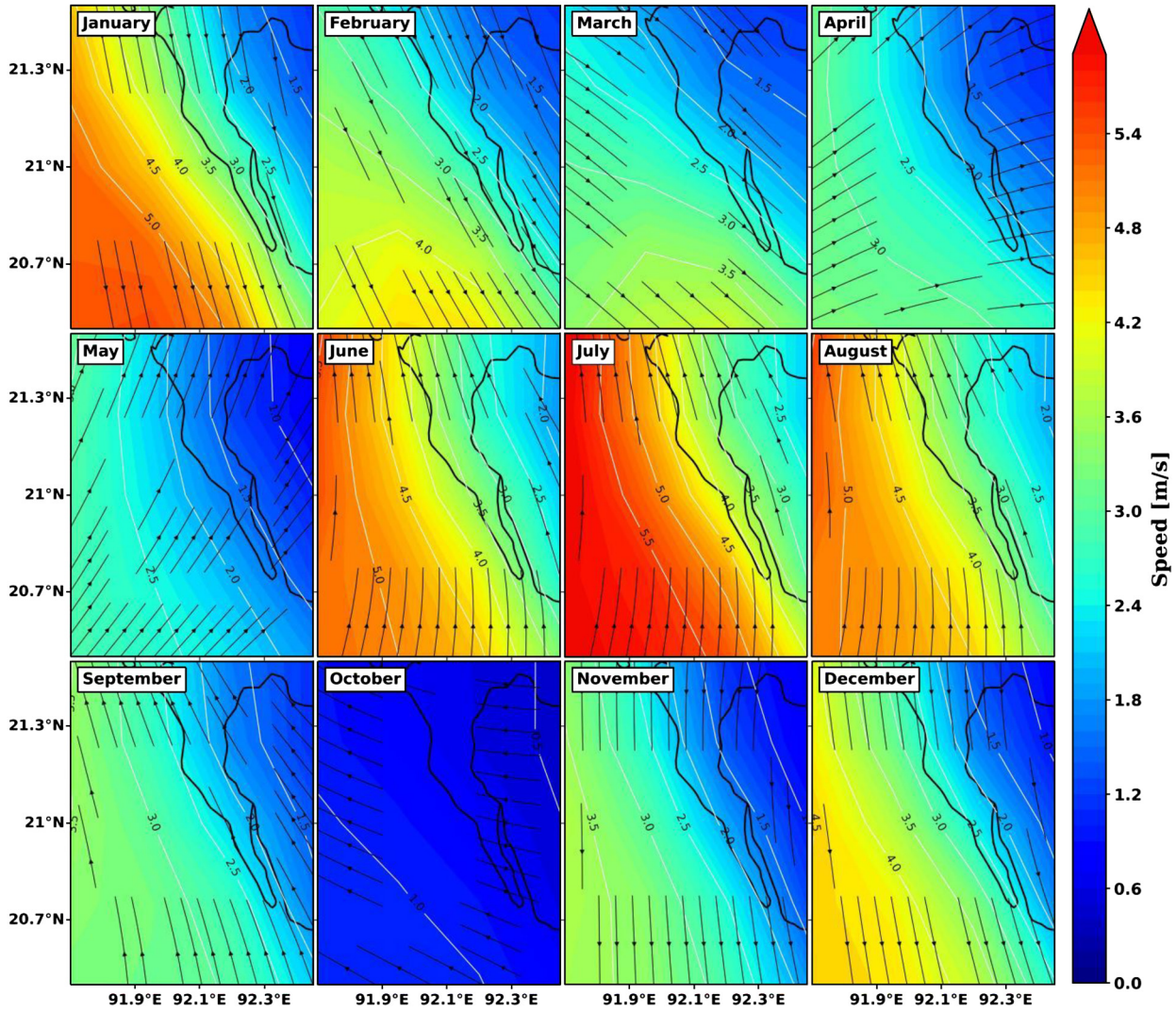

Table 13
Yearly precipitation (mm) values from 2015 to 2024 based on both secondary sources and BMD data

	Yearly precipitation (mm) of 2015–2024									
Data sources	**2015**	**2016**	**2017**	**2018**	**2019**	**2020**	**2021**	**2022**	**2023**	**2024**
Secondary data	2666.3	2528.4	2678.5	2234.0	2187.7	2629.5	2351.2	1952.9	2289.7	2768.8
BMD data	5081.5	3798.0	4064.5	3781.0	3376.5	4000.5	3263.0	2346.0	2414.5	3467.8

datasets but also the noticeable year-to-year variations in rainfall across the region during the 10-year period.

3.5.3. Trend analysis of precipitation

Figure 19 shows two-line graphs that compare monthly or short-term total rainfall from 2015 to 2024 using two different sources: one based on secondary data (a) and the other from BMD records (b). In the graph using secondary data, rainfall levels vary noticeably throughout the year, with clear spikes during the monsoon months, reflecting the seasonal nature of precipitation in the region. In 2015, the secondary data show a sharp peak where rainfall exceeds 800 mm in a single period. Similarly high values appear in later years, such as over 700 mm in both 2019 and 2021. The driest months in each year show rainfall decreasing to nearly zero. Conversely, the BMD data also show clear seasonal shifts, with even higher rainfall totals during the monsoon. In some years such as 2015 and 2017, single-period rainfall crosses 1200 mm. Dry periods in the BMD data similarly show very low rainfall, close to zero. Overall, both graphs reflect the strong seasonal nature of rainfall in the region, marked by heavy monsoon rains and much drier intervals, and highlight noticeable differences in the rainfall amounts reported by the two sources.

Figure 17
Seasonal spatiotemporal distribution of wind speed (m/s) in the Cox's Bazar–Teknaf region from 2015 to 2024. Wind vectors indicate wind direction, providing a comprehensive view of seasonal wind patterns

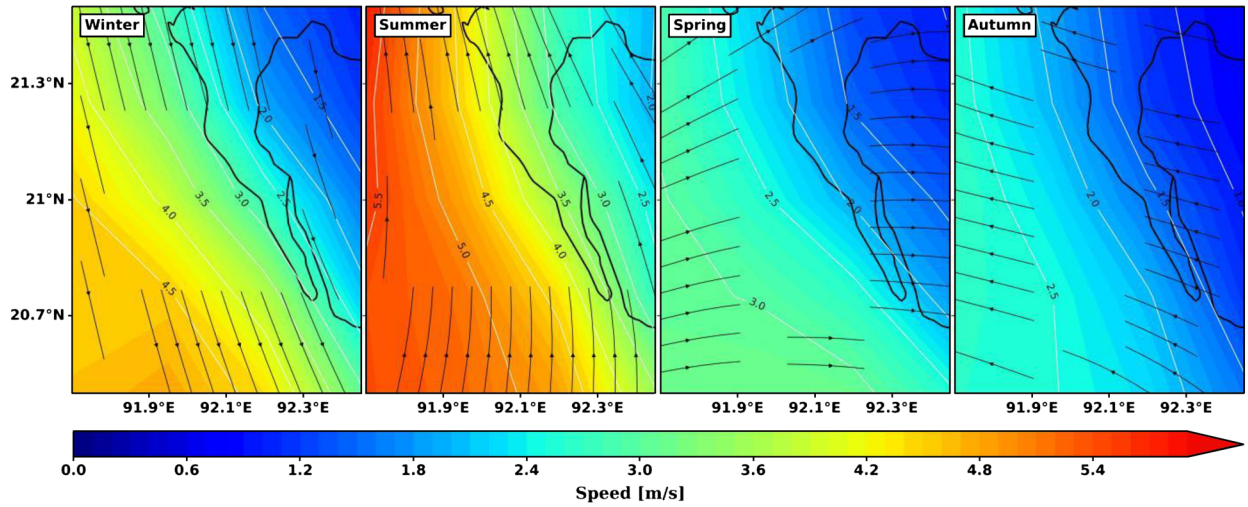

Figure 18
Yearly spatiotemporal distribution of precipitation (mm) in the Cox's Bazar–Teknaf region from 2015 to 2024

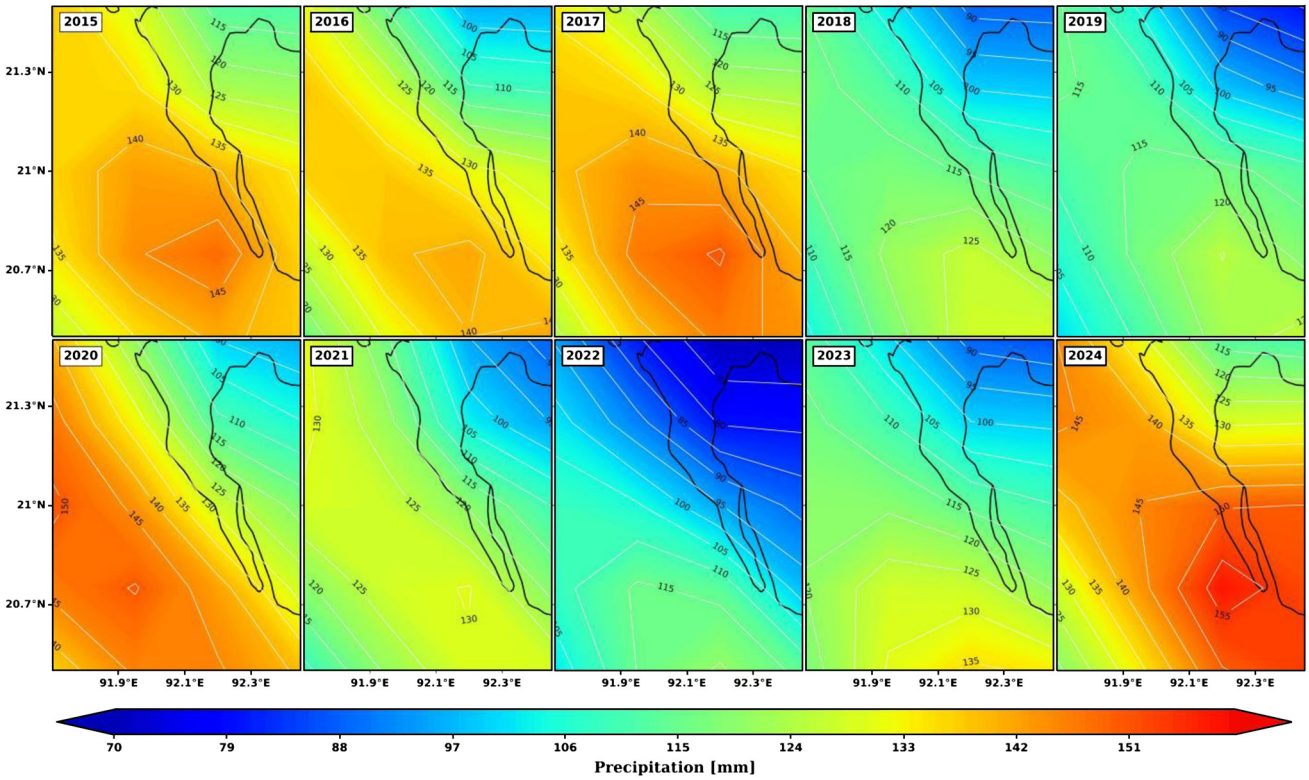

3.5.4. Monthly climatology of precipitation

Figure 20 illustrates average monthly precipitation data, likely from 2015 to 2024, presented as a series of contour maps for each month. Each map uses color shading to represent rainfall amounts in millimeters, with shades from yellow to red indicating higher rainfall levels within a range of 0–36 mm, as noted on the color scale to the right. From January to March, rainfall remains minimal across the region, with most areas receiving less than 4 mm, shown in blue shades. As the season moves into April and May, precipitation gradually increases, especially in May, where some zones record approximately 8–12 mm, reflected in light green to yellow tones. The heaviest rainfall occurs in June and July, with July reaching up to 32–36 mm in certain locations, highlighted in orange and red. Rainfall stays relatively high in August but starts to decrease in September, with totals decreasing to approximately 16–24 mm. By October and November, the region sees further reduction in rainfall, averaging between 8 and 16 mm, and

Figure 19
Time series analysis of precipitation (mm) from 2015 to 2024. (a) Secondary data and (b) BMD data illustrate decadal fluctuations over time

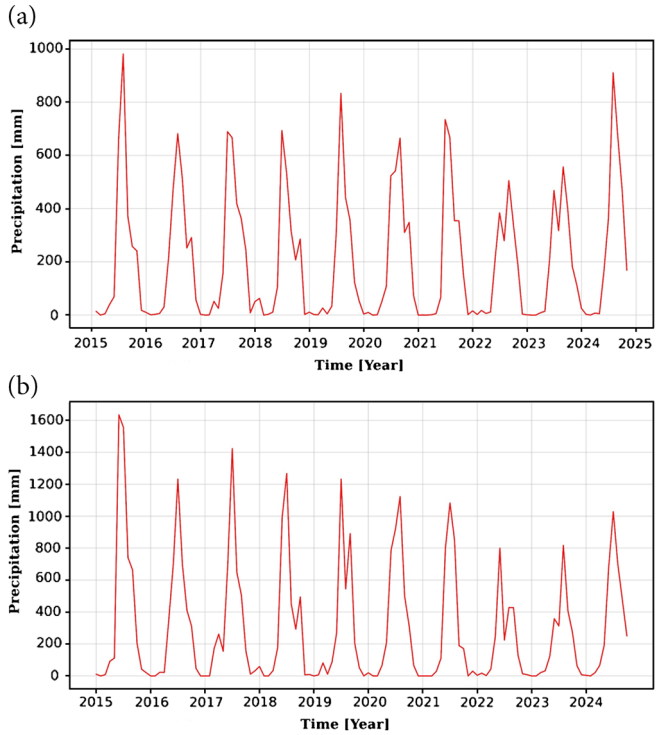

December marks a return to very low levels similar to early in the year. This sequence clearly illustrates the seasonal rhythm of precipitation, with a pronounced peak in the summer and noticeably drier periods at the beginning and end of the year.

3.5.5. Monthly mean of precipitation

Table 14 presents the monthly mean precipitation values from 2015 to 2024 based on two different data sources: secondary data and BMD data. In the secondary data chart, July experiences the highest mean precipitation at 641.8 mm, followed by June at 530.0 mm and August at 481.5 mm. Other months show significantly lower values, with May at 134.1 mm, April at 19.6 mm, March at 11.6 mm, January at 9.5 mm, February at 2.2 mm, December at 13.4 mm, November at 36.8 mm, September at 331.3 mm, and October at 222.0 mm. Conversely, in the BMD data chart, July has the highest mean precipitation at 1027.9 mm, followed by June at 772.8 mm and August at 699.7 mm. Other months also reflect generally higher values compared to the secondary data, with September at 476.2 mm, May at 176.4 mm, April at 65.4 mm, March at 32.8 mm, January at 9.7 mm, February at 2.4 mm, December at 11.8 mm, November at 33.5 mm, and October at 250.7 mm. The BMD data show a more pronounced peak in July and generally higher precipitation across most months, indicating substantial rainfall variability and differences in reporting between the two sources. This comparison effectively highlights the seasonal distribution of precipitation across the months and the differences between the datasets.

3.5.6. Spatial distribution of seasonal precipitation

Figure 21 shows average seasonal rainfall across winter, spring, summer, and autumn, likely covering the years 2015 to 2024, using contour maps. During winter, rainfall is minimal, with most areas getting less than 3.5 mm, shown in dark blue. Spring brings a slight increase, with rainfall ranging from approximately 3.5 to 10.5 mm, marked by blue to light green shades. In summer, rainfall increases sharply, reaching up to 31.5 mm in some places, especially where orange and red colors appear. Autumn sees a decrease again, with rainfall between approximately 7 and 17.5 mm, shown in green to yellow tones. Overall, the maps clearly highlight how rainfall peaks during summer, and winter and spring remain much drier.

3.5.7. Seasonal mean of precipitation

Table 15 presents the seasonal average precipitation in the Cox's Bazar–Teknaf region from 2015 to 2024 based on secondary data and BMD records. In the secondary dataset, rainfall peaks in summer at 551.1 mm, and winter is the driest season with only 8.2 mm. Spring and autumn receive 55.1 and 202.2 mm, respectively. The BMD data show even higher totals, with summer rainfall reaching 833.5 mm, compared to 8.0 mm in winter, 91.5 mm in spring, and 253.5 mm in autumn. Both datasets highlight strong seasonal contrasts, with summer bringing the heaviest rainfall, particularly evident in the BMD records.

3.5.8. EOF analysis

Figure 22 shows the first principal component (PC1) of the atmospheric variables in the study area, accounting for 99% of the total variance and clearly reflecting a dominant seasonal cycle.

The PC1 time series (top panel) shows positive amplitudes from May to September (monsoon period) and negative amplitudes from November to March (dry season), indicating a clear shift in atmospheric conditions. Spatial patterns for each variable (bottom panels) reveal that air temperature and relative humidity are higher during the monsoon months, and surface pressure is relatively lower. Zonal and meridional wind patterns exhibit distinct directional changes linked to monsoon onset and withdrawal. Precipitation intensity peaks in the central and

Table 15
Seasonal average precipitation (mm) values from 2015 to 2024 based on both secondary sources and BMD data

Seasonal mean precipitation (mm) of 2015–2024				
Data sources	**Winter**	**Summer**	**Spring**	**Autumn**
Secondary data	8.2	551.1	55.1	202.2
BMD data	8.0	833.5	91.5	253.5

Table 14
Monthly average precipitation (mm) values from 2015 to 2024 based on both secondary sources and BMD data

Monthly mean precipitation (mm) of 2015–2024												
Data sources	**Jan**	**Feb**	**Mar**	**Apr**	**May**	**Jun**	**Jul**	**Aug**	**Sept**	**Oct**	**Nov**	**Dec**
Secondary data	9.5	2.2	11.6	19.6	134.1	530.0	641.8	481.5	331.3	222.0	36.8	13.4
BMD data	9.7	2.4	32.8	65.4	176.4	772.8	1027.9	699.7	476.2	250.7	33.5	11.8

Figure 20
Monthly spatiotemporal distribution of precipitation (mm) in the Cox's Bazar–Teknaf region from 2015 to 2024

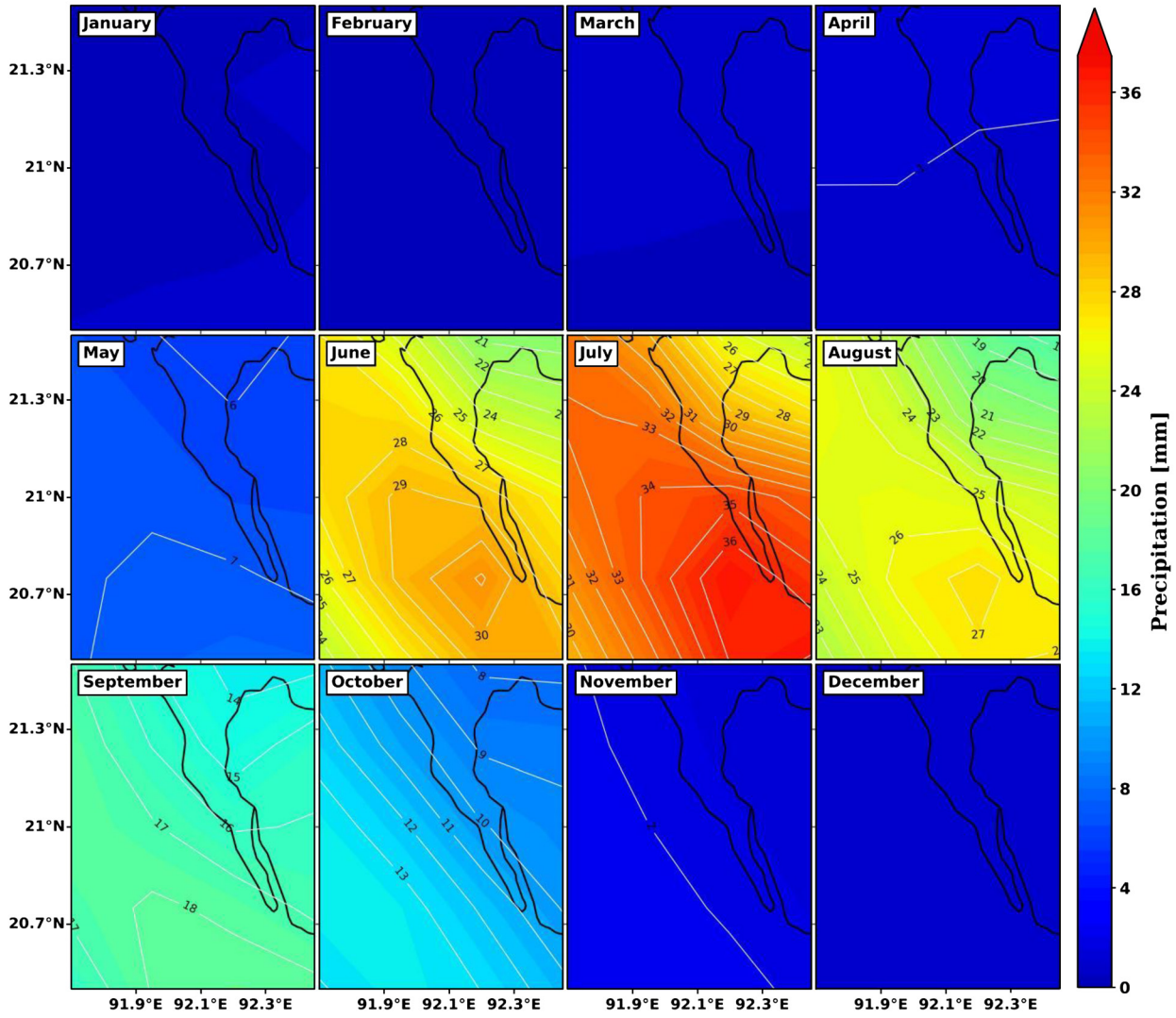

Figure 21
Seasonal spatiotemporal distribution of precipitation (mm) in the Cox's Bazar–Teknaf region from 2015 to 2024

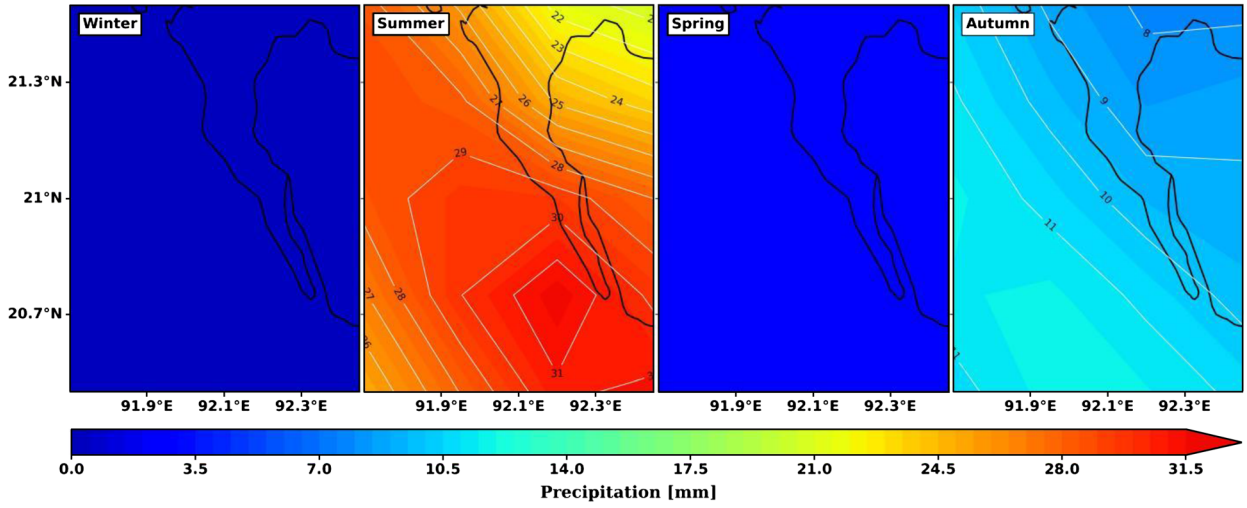

Figure 22

PC1 analysis of atmospheric variables over the study region, explaining 99% of the total variance. (Top) Seasonal cycle of PC1 amplitude across months. (Bottom) Spatial patterns for air temperature, surface pressure, relative humidity, zonal wind, meridional wind, and precipitation, highlighting seasonal contrasts between dry and monsoon periods

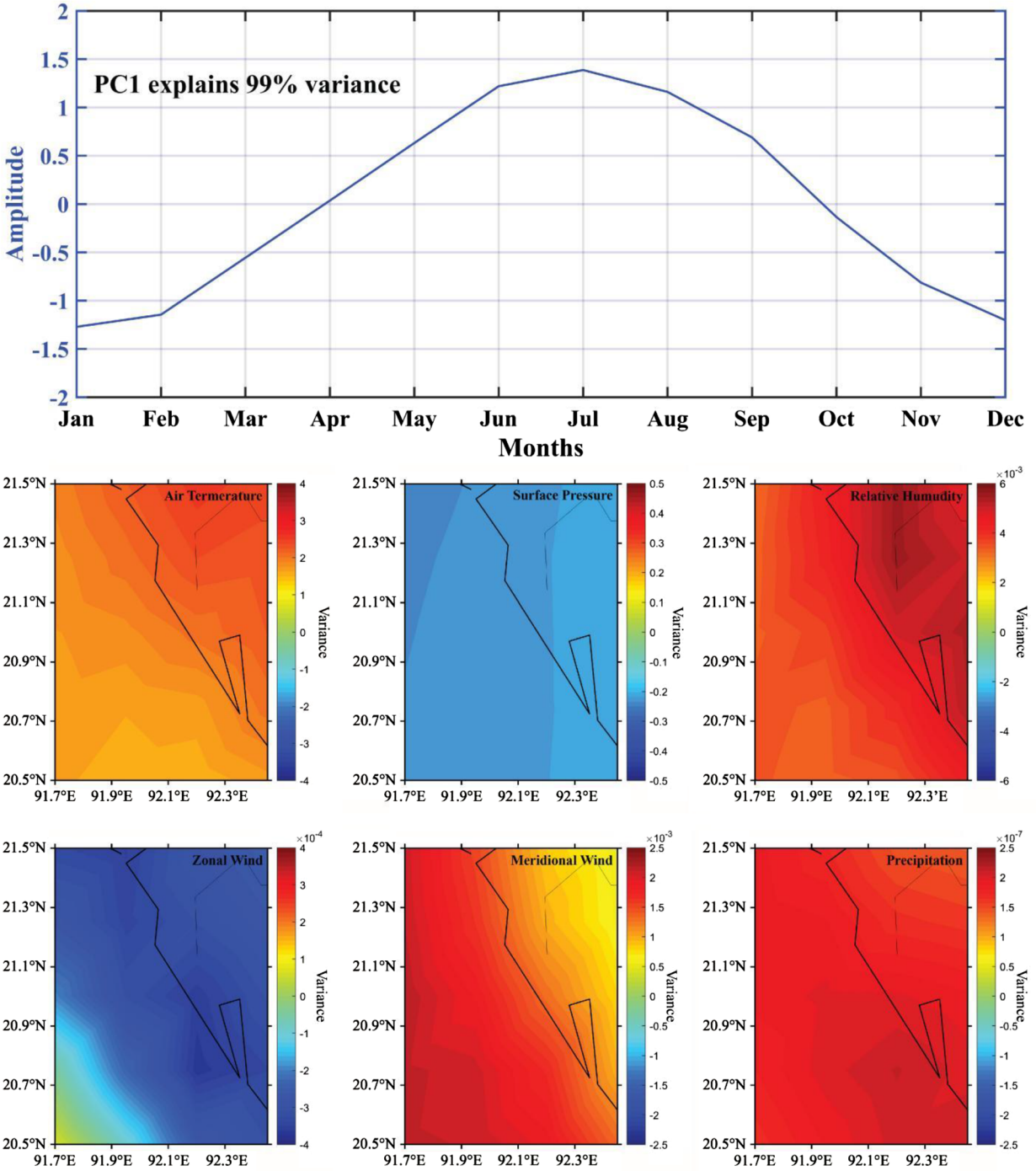

eastern parts during the wet season, correlating with wind-driven moisture transport.

3.5.9. Correlation and regression analysis

Figure 23 presents the correlation matrix and regression fits among key atmospheric parameters over the study region. Each scatterplot shows the relationship between two variables, with red lines representing linear regression fits. The correlation coefficients (R) are shown in each panel, with their significance levels in brackets. Strong negative correlations are observed between surface pressure and air temperature (R = −0.59), surface pressure and relative humidity (R = −0.56), and surface pressure and meridional wind (R = −0.72), indicating that low-pressure conditions are associated with higher temperatures, increased humidity, and stronger meridional winds.

Figure 23

Pairwise correlation and regression fit among air temperature, surface pressure, precipitation, relative humidity, zonal wind, and meridional wind. Scatterplots show data points (blue) with linear regression lines (red). Correlation coefficients (R) and p-values are indicated in each panel, revealing significant positive and negative relationships that describe the coupled atmospheric processes in the study area

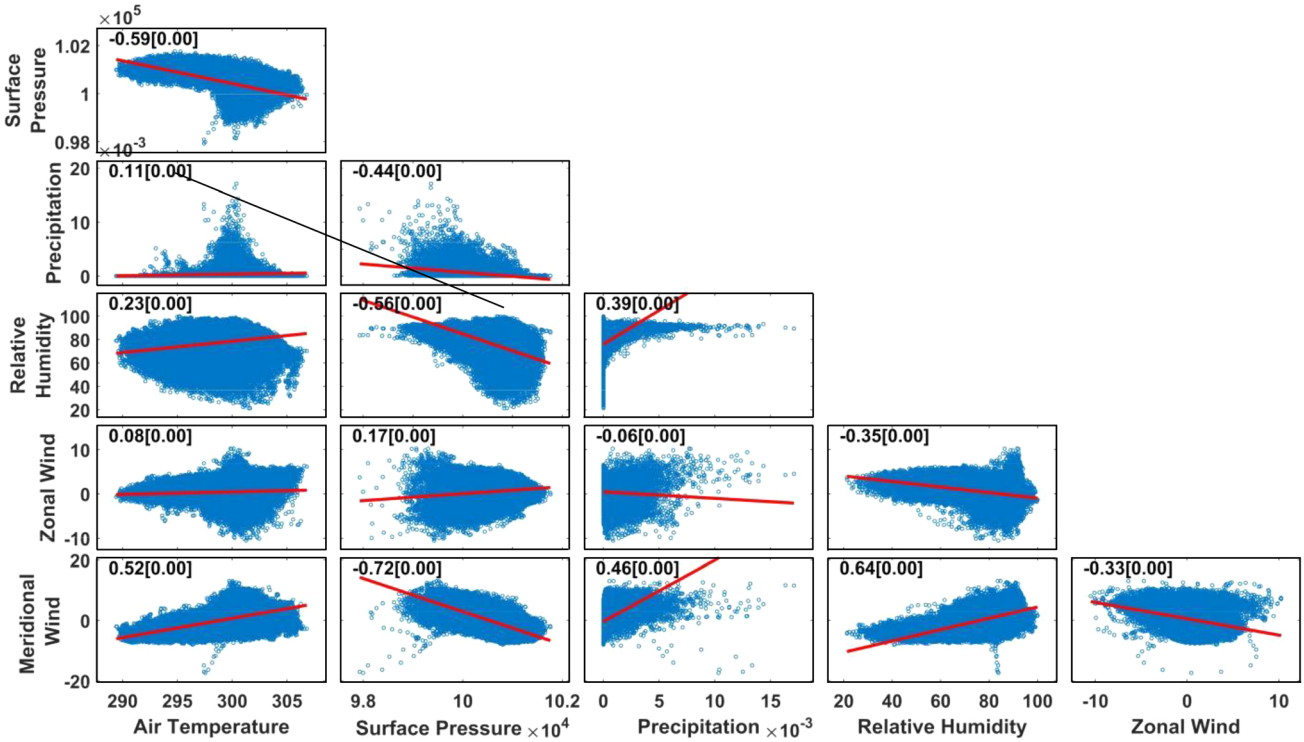

Conversely, a strong positive correlation exists between meridional wind and relative humidity (R = 0.46) and between meridional and zonal winds (R = 0.64), reflecting wind coupling during monsoon circulation. These relationships highlight the interconnected nature of atmospheric dynamics over the BoB.

4. Discussion

Weather patterns play a decisive role in shaping the socio-economic conditions of the southeastern coastal region of Bangladesh. As part of the Ganges–Brahmaputra delta in northeastern South Asia, this low-lying area of flat terrain and extensive floodplains is highly exposed to sea-level rise, cyclones, storm surges, and seasonal flooding [8, 9, 15]. As a developing country heavily dependent on agriculture and fishing, Bangladesh is particularly vulnerable to climate variability [16]. These challenges are most pronounced along the Cox's Bazar–Teknaf coastal stretch, where climate-related threats and natural disasters pose serious risks to local communities. Similar vulnerabilities are reported in other deltaic regions, such as Vietnam and the Philippines, where low-lying coastal areas face increasing flood and cyclone risks [17, 18].

The study region is characterized by a subtropical monsoon climate with four distinct seasons: winter (December–February), pre-monsoon summer (March–May), the rainy season (June–September), and post-monsoon autumn (October–November) [19]. Average annual temperatures range from 25°C to 30°C, with January as the coldest month and April as the hottest [20]. More than 80% of the average annual rainfall of 2768.8 mm occurs during the rainy season, accompanied by high relative humidity averaging 80% [21]. This strong seasonality makes the ecosystem highly sensitive to even minor changes in precipitation and temperature. Our analysis reveals a consistent increase in air temperature, associated with more frequent extreme weather events, which corresponds with broader climate shifts observed across the BoB. These findings align with earlier studies documenting increasing cyclone frequency and shifting rainfall patterns [8, 22–24]. High-resolution temperature and rainfall maps thus provide valuable tools for climate-smart agriculture and socio-economic resilience [6], and similar monsoonal trends have been reported in Sri Lanka and southern India [25].

The observed climate variability has direct socio-economic implications. Shifting rainfall patterns and increasing temperatures affect agriculture, fisheries, and tourism, the three key economic pillars of this region. Farmers are compelled to modify planting and harvesting schedules, fishermen face changes in fish availability and breeding linked to altered oceanic conditions, and the tourism industry, especially in Cox's Bazar and Saint Martin's Island, relies on stable seasonal weather for visitor safety and comfort [26]. By linking these sectoral outcomes to weather variability, this study emphasizes the importance of integrating climate data into both short-term adaptation measures and long-term resilience strategies. Global warming amplifies these challenges: since pre-industrial times, global temperatures have increased by approximately 0.99°C, with projections of a 1°C–3°C increase by the century's end [11]. Such warming is expected to intensify floods, droughts, cyclones, and rainfall variability [9], posing a direct threat to agriculture, fisheries, and tourism in the Cox's Bazar–Teknaf belt [16]. The evidence presented here confirms earlier warnings regarding the vulnerability of deltaic regions and underscores the urgency of proactive adaptation planning.

Globally, there is a growing agreement that developing countries, particularly in South Asia, will play a critical role in addressing energy crisis and environmental challenges [27]. As the energy demand in these regions increases and approaches levels of developed nations, reliance

on fossil fuels intensifies resource pressures, accelerating global warming and greenhouse gas emissions [28, 29]. In response, many countries are shifting toward renewable energy sources, particularly solar and wind, to reduce emissions and strengthen climate resilience [28, 30]. Comparable transitions are evident in Indonesia and Thailand, where coastal wind and solar resources are being harnessed to improve energy security [31, 32]. For Bangladesh, limited potential exists for fuel cells and geothermal, tidal, or wave energy [26], making wind energy an especially promising option alongside solar and biomass. The analysis of the wind characteristics between 2015 and 2024 shows monthly average wind speeds ranging from 2.4 m/s in November to 4.5 m/s in July, with the highest seasonal average of 4.13 m/s during summer (Table 11). The monthly shape factor varied from 4.73 to 9.24, and the scale parameter ranged between 2.50 and 2.98 m/s. Seasonal averages ranged from 1.89 m/s in autumn to 4.13 m/s in summer (Table 12), highlighting the feasibility of wind turbine installation along the Cox's Bazar–Teknaf coast [7]. Similar assessments in Pakistan's Makran coast and India's Odisha coast also demonstrate substantial wind energy potential, further justifying regional investment in coastal renewable energy [33, 34].

Renewable energy offers a dual opportunity to mitigate climate risks and enhance resilience. It offers a cleaner alternative to fossil fuels by significantly reducing carbon dioxide emissions, one of the major drivers of climate change [28]. Among renewable sources, solar and wind are particularly suitable for both grid-connected and remote applications [16]. With technological advancements, wind energy conversion technologies (WECT) have become increasingly efficient, making wind one of the fastest-growing renewable energy sources worldwide [27]. Over the past decade, the global adoption of wind power has expanded significantly: by 2011, wind energy was commercially utilized in 83 countries, and global capacity had nearly doubled every 2.5 years [19]. For instance, worldwide wind capacity increased from 93,930 MW in 2007 to 197,637 MW in 2010, with Europe contributing the largest share of these installations [30, 35]. Countries such as Denmark, Portugal, Spain, Ireland, and Germany have achieved high penetration rates of wind power, demonstrating its viability as a mainstream energy option [29].

In addition, this study provides crucial insights that go beyond just climate science using detailed weather datasets. It also offers direct, practical applications for socio-economic development and long-term resilience planning. The comprehensive data that we analyzed included temperature (Table 1), precipitation (annual trends in Table 13, monthly trends in Table 14, and seasonal patterns in Figure 21), relative humidity (annual trends in Figure 10 and Table 7, monthly trends in Figure 12 and Table 8, and seasonal variations in Figure 13 and Table 9), and wind speed (Figures 14, 15, 16, and 17 and Tables 10, 11, and 12).

These findings offer actionable insights for various sectors, including agriculture, fisheries, tourism, disaster preparedness, renewable energy, and public health [10]. Temperature and rainfall forecasts can help farmers make smarter decisions regarding planting and irrigation, which, in turn, reduces crop losses [16]. By understanding precipitation patterns (Figures 18 and 20) and seasonal temperature shifts (Figure 5), we can improve yield forecasts and promote climate-smart farming techniques [20]. Fishermen can use these data to identify optimal times and locations for fishing. In addition, trends in rainfall and surface pressure (Figure 8) provide a way to monitor changes in the marine environment that affect fish behavior and breeding patterns [7]. Understanding seasonal variations in humidity and rainfall is vital for tourism and local planning, especially in popular coastal areas such as Cox's Bazar and Saint Martin's Island. This information can improve visitor safety and boost economic performance [6, 26]. Weather patterns are closely linked to public health. Changes in temperature and precipitation, for example, can directly influence the spread of diseases such as dengue and malaria [36]. Our findings align with similar research in Tanzania and the Caribbean, which shows that integrating weather data into coastal management significantly improves resilience across agriculture, fisheries, and tourism [37, 38].

Furthermore, the EOF analysis performed in this study revealed the dominant modes of variability in the atmospheric parameters across the southeastern coastal region of Bangladesh. The first principal component (PC1) alone explained 99% of the total variance, strongly indicating seasonal cycles in temperature, wind, pressure, humidity, and precipitation. This dominant seasonal signal is tied to the monsoonal transition, with high activity in summer and low activity in winter [12]. The correlation and regression analyses among the parameters provided additional insights into the coupled dynamics of the local climate system. For instance, a strong negative correlation between surface pressure and temperature, humidity, and meridional wind suggests that low-pressure systems typically bring warm, humid, and windy monsoon conditions. Furthermore, positive correlations among winds and humidity show how winds play a critical role in bringing moisture from the BoB inland. These results provide a solid scientific basis for creating better predictive models, early warning systems, and climate-resilient plans [12]. Comparable studies in China's Pearl River Delta and East African coasts confirm the global relevance of these findings [39, 40]. The combination of EOF and correlation analyses not only enhances our understanding of atmospheric variability but also helps in developing more robust predictive models for agricultural planning, disaster preparedness, and renewable energy optimization along the Cox's Bazar–Teknaf coastal belt.

Bangladesh ranks as the seventh most climate-vulnerable country according to the Global Climate Risk Index 2021 [1]. The southeastern coast is frequently hit by natural disasters such as cyclones, floods, and heavy rainfall, which are often caused by recurring low-pressure systems and cyclonic activity. These events severely disrupt local infrastructure, livelihoods, and economic growth [10]. To adapt, it is crucial to strengthen early warning systems, improve water management, and build more resilient infrastructure [9, 15, 21, 41]. Our analysis of annual and seasonal trends in rainfall and surface pressure (Figures 8 and 9) is especially important for water resource management in a river-dependent country such as Bangladesh [21]. This information can help in ensuring a reliable water supply for farming, domestic use, and industry [16]. By studying long-term patterns in temperature (Figure 3) and rainfall (Figure 19), we can also guide the construction of durable roads, bridges, and housing that can withstand harsh weather conditions [15]. Effective disaster preparedness can even attract international support and investment for climate-resilient infrastructure [27]. Experiences from the Philippines and Mozambique show that better monitoring of rainfall and pressure patterns significantly improves community preparedness and resilience [41, 42].

Altogether, this study highlights that using high-resolution data and robust analytical methods to understand climate variability is essential for creating effective, multisectoral adaptation strategies. This information can empower policymakers and planners to design and implement solutions that reduce climate-related risks, such as promoting afforestation and other long-term measures [9]. By turning observed climate trends into practical insights, this study provides a clear path to improve agricultural productivity, fishery sustainability, tourism planning, disaster preparedness, and renewable energy development. This, in turn, will contribute to the long-term socio-economic and environmental resilience of this vulnerable coastal region.

4.1. Limitations of the study

Every research project has its limitations, and ours is no exception. First, the analysis uses a mixture of reanalysis, satellite, and ground-based datasets. Although authors did everything possible to ensure the quality and consistency of these data, some uncertainties remain. This is particularly true for areas where we had few ground-based observations, which can leave small, lingering errors from the different data acquisition methods. Second, authors had to use interpolation to fill in spatial and temporal gaps. This process is great for creating a continuous dataset, but it can smooth over localized extreme weather events, which might slightly affect the accuracy of the fine-scale variability. Third, this study focuses on a decade-long period (2015–2024). Although this timeframe is excellent for capturing recent trends, it may not be long enough to fully represent long-term climate variability or the multidecadal cycles of the region. Fourth, the methods that we used, such as EOF analysis and correlation, are very effective for finding dominant patterns and relationships among variables, but these do not prove a cause-and-effect relationship. Understanding the full influence of complex ocean–atmosphere interactions, for example, would require more advanced modeling than we could conduct. Finally, the scope of this study is primarily meteorological. A more comprehensive picture of coastal community resilience would need to integrate a full assessment of socio-economic and ecological impacts, which was beyond the scope of this study.

5. Conclusion

This study emphasizes the importance of high-resolution weather data for managing the Cox's Bazar–Teknaf coastal zone, one of Bangladesh's most climate-sensitive regions. Exposed to rising sea levels, cyclones, and seasonal flooding, the area urgently requires accurate and long-term environmental monitoring. By analyzing the spatiotemporal patterns of air temperature, humidity, wind speed, surface pressure, and precipitation, this study identifies key trends that influence local ecosystems and livelihoods and addresses a major gap in regional climate studies.

The results point to a steady warming trend, more frequent extreme weather events, and clear seasonal shifts in rainfall, underscoring the need for adaptive coastal management. The use of EOF analysis, together with correlation, regression, and trend testing, provides a strong basis for identifying dominant climate patterns and the interconnections among weather processes. The assessment of the wind energy potential further highlights opportunities for renewable energy development, supporting both energy security and climate resilience.

The maps and visual outputs developed here offer practical value for policymakers by supporting disaster preparedness, climate-responsive resource planning, and informed decision-making. Key recommendations include integrating high-resolution weather monitoring into early warning systems, aligning agricultural and fisheries planning with seasonal rainfall variability, piloting wind energy initiatives in promising areas, and embedding spatiotemporal climate analysis into coastal management policies.

By linking observed climate variability to actionable strategies for governance, risk reduction, and sustainable development, this study not only advances scientific understanding but also provides a framework for future adaptation. Ongoing monitoring and systematic application of these insights in local planning will be essential to strengthen the long-term resilience and sustainability of the Cox's Bazar–Teknaf coast.

Recommendations

On the basis of the analysis of decadal weather trends, several measures are recommended to strengthen coastal resilience and support sustainable development in the Cox's Bazar–Teknaf region. First, localized early warning systems with real-time weather data should be implemented to improve disaster preparedness and response. Second, the development of renewable energy, particularly wind power in areas with favorable seasonal conditions, should be encouraged to enhance energy security and reduce carbon emissions. In addition, observed climate trends need to be incorporated into coastal infrastructure planning, especially in tourism-prone areas, to minimize risks from sea-level rise, coastal erosion, and storm surges. Promoting climate-resilient agricultural practices that align with seasonal patterns of temperature, rainfall, and humidity is also essential for safeguarding local livelihoods. Finally, a stronger collaboration among agencies is required to improve the use of geospatial weather and climate data, ensuring more effective policymaking and long-term adaptation strategies.

Acknowledgement

We would like to express our sincere gratitude to the Copernicus Marine Environment Monitoring Service (CMEMS) for providing the essential data, the Climate Data Store for atmospheric data, and the Bangladesh Meteorological Department (BMD) in situ data that made this study possible. Special thanks to our colleagues, mentors, and institutions for their continuous support and insightful feedback throughout this study. Finally, we acknowledge the use of Python programming tools and GIS software, which facilitated our data processing and visualization efforts.

Ethical Statement

This study does not contain any studies with human or animal subjects performed by any of the authors.

Conflicts of Interest

The authors declare that they have no conflicts of interest to this work.

Data Availability Statement

The datasets used and analyzed in this study are publicly available from the Copernicus Climate Data Store (CDS-ERA5: https://cds.climate.copernicus.eu/) and the Bangladesh Meteorological Department (BMD: https://dataportal.bmd.gov.bd/). Processed datasets and plots are available upon reasonable request from the corresponding author.

Author Contribution Statement

Siraj Uddin Md Babar Chowdhury: Conceptualization, Methodology, Software, Validation, Formal analysis, Investigation, Resources, Data curation, Writing – original draft, Visualization, Supervision, Project administration. **Anik Karmakar:** Methodology, Software, Validation, Formal analysis, Investigation, Resources, Data curation, Writing – original draft, Visualization, Supervision, Project administration. **K. M. Azam Chowdhury:** Conceptualization, Methodology, Software, Validation, Formal analysis, Resources,

Data curation, Writing – original draft, Visualization, Supervision, Project administration. **Tabassum Hossain Tahsin:** Investigation, Writing – review & editing. **Abdullah Al Mamun Siddiqui:** Validation, Resources, Writing – review & editing, Supervision. **Tasin Sumaia Khan:** Investigation, Resources, Data curation, Writing – review & editing, Visualization. **Mohammad Rokan Uddin:** Validation, Resources, Writing – original draft, Writing – review & editing, Visualization.

References

[1] Eckstein, D., Künzel, V., & Schäfer, L. (2021). *Global climate risk index 2021*. Germanwatch. https://www.germanwatch.org/en/19777

[2] Islam, A., Islam, M. S., Hasan, M., & Khan, A. H. (2013). Analysis of wind characteristics and wind energy potential in coastal area of Bangladesh: Case study – Cox's Bazar. *ELEKTRIKA*, *15*(2), 1–10.

[3] Shaw, R., Mallick, F., & Islam, A. (Eds.). (2013). *Disaster risk reduction approaches in Bangladesh*. Japan: Springer.

[4] Wu, Y., Yang, J., Zhang, Z., Das, L. C., & Crabbe, M. J. C. (2024). High-resolution temperature evolution maps of Bangladesh via data-driven learning. *Atmosphere*, *15*(3), 385. https://doi.org/10.3390/atmos15030385

[5] Roy, S., Saha, M., Hasan, M. M., Razzaque, A., Sumaiya, N., Hoque, M. A. A., …, & Depellegrin, D. (2024). Multi-pressure based environmental vulnerability assessment in a coastal area of Bangladesh: A case study on Cox's Bazar. *Geomatica*, *76*(2), 100030. https://doi.org/10.1016/j.geomat.2024.100030

[6] Rakib, M. R. J., Hossain, M. B., Islam, M. S., Hossain, I., Rahman, M. M., Kumar, R., & Sharma, P. (2022). Ecohydrological features and biodiversity status of estuaries in Bengal delta, Bangladesh: A comprehensive review. *Frontiers in Environmental Science*, *10*, 990099. https://doi.org/10.3389/fenvs.2022.990099

[7] Islam, N., Iqra, S. A., Huq, A. S., & Tasnim, A. (2023). An econometric analysis of weather effects on roadway crash severity in Bangladesh: Evidence from the Dhaka metropolitan area. *Sustainability*, *15*(17), 12797. https://doi.org/10.3390/su151712797

[8] Chowdhury, S. U. M. B., Karmakar, A., Hoque, M. E., Hoque, M. M., Tahsin, T. H., & Chowdhury, S. (2025). Upper ocean response mechanisms to pre-monsoon and post-monsoon cyclones in the Bay of Bengal. *Ocean-Land-Atmosphere Research*, *4*, 0105. https://doi.org/10.34133/olar.0105

[9] Huq, S., & Rabbani, G. (2011). Climate change and Bangladesh: Policy and institutional development to reduce vulnerability. *Journal of Bangladesh Studies*, *13*(1), 1–10. https://doi.org/10.1163/27715086-01301002

[10] Ahmed, S., & Khan, M. A. (2023). Spatial overview of climate change impacts in Bangladesh: A systematic review. *Climate and Development*, *15*(2), 132–147. https://doi.org/10.1080/17565529.2022.2062284

[11] Skea, J., Shukla, P., Al Khourdajie, A., & McCollum, D. (2021). Intergovernmental Panel on Climate Change: Transparency and integrated assessment modeling. *WIREs Climate Change*, *12*(5), e727. https://doi.org/10.1002/wcc.727

[12] Chowdhury, S. U. M. B., Chowdhury, N. U. M. K., Chowdhury, K. A., Karmakar, A., & Tahsin, T. H. (2025). Spatiotemporal variability of seawater density profile and nitrate productivity in the Bay of Bengal. *Regional Studies in Marine Science*, *86*, 104214. https://doi.org/10.1016/j.rsma.2025.104214

[13] Emery, W. J., & Thomson, R. E. (2004). *Data analysis methods in physical oceanography* (second and revised edition). Netherlands: Elsevier.

[14] Wilks, D. S. (2011). *Statistical methods in the atmospheric sciences* (Vol. 100). Netherlands: Academic Press; Elsevier.

[15] Rahman, S., Islam, A. S., Saha, P., Tazkia, A. R., Krien, Y., Durand, F., …, & Bala, S. K. (2019). Projected changes of inundation of cyclonic storms in the Ganges–Brahmaputra–Meghna delta of Bangladesh due to SLR by 2100. *Journal of Earth System Science*, *128*(6), 145. https://doi.org/10.1007/s12040-019-1184-8

[16] Hossain, M. S., Arshad, M., Qian, L., Zhao, M., Mehmood, Y., & Kächele, H. (2019). Economic impact of climate change on crop farming in Bangladesh: An application of Ricardian method. *Ecological Economics*, *164*, 106354. https://doi.org/10.1016/j.ecolecon.2019.106354

[17] Rehman, S., Azhoni, A., & Chabbi, P. H. (2023). Livelihood vulnerability assessment and climate change perception analysis in Arunachal Pradesh, India. *GeoJournal*, *88*(2), 1427–1447. https://doi.org/10.1007/s10708-022-10703-7

[18] Nguyen, T., Brandstetter, J., Kapoor, A., Gupta, J. K., & Grover, A. (2023). ClimaX: A foundation model for weather and climate. In *Proceedings of the 40th International Conference on Machine Learning*, 25904–25938.

[19] Islam, A. R. M. T., Nafiuzzaman, M., Rifat, J., Rahman, M. A., Chu, R., & Li, M. (2020). Spatiotemporal variations of thunderstorm frequency and its prediction over Bangladesh. *Meteorology and Atmospheric Physics*, *132*(6), 793–808. https://doi.org/10.1007/s00703-019-00720-6

[20] Ahmad, Q. K., Warrick, R. A., Ericksen, N. J., & Mirza, M. Q. (1996). The implications of climate change for Bangladesh: A synthesis. In R. A. Warrick & Q. K. Ahmad (Eds.), *The implications of climate and sea-level change for Bangladesh* (pp. 1–34). Springer. https://doi.org/10.1007/978-94-009-0241-1_1

[21] Shahid, S. (2010). Rainfall variability and the trends of wet and dry periods in Bangladesh. *International Journal of Climatology*, *30*(15), 2299–2313. https://doi.org/10.1002/joc.2053

[22] Rahman, S., Sharmin, N., Rahat, A., Rahman, M., & Rahman, M. (2024). Tropical cyclone warning and forecasting system in Bangladesh: Challenges, prospects, and future direction to adopt artificial intelligence. *Computational Urban Science*, *4*(1), 4. https://doi.org/10.1007/s43762-023-00113-x

[23] Naidu, P. D., Ganeshram, R., Bollasina, M. A., Panmei, C., Nürnberg, D., & Donges, J. F. (2020). Coherent response of the Indian monsoon rainfall to Atlantic multi-decadal variability over the last 2000 years. *Scientific Reports*, *10*(1), 1302. https://doi.org/10.1038/s41598-020-58265-3

[24] Langer, J., Quist, J., & Blok, K. (2021). Review of renewable energy potentials in Indonesia and their contribution to a 100% renewable electricity system. *Energies*, *14*(21), 7033. https://doi.org/10.3390/en14217033

[25] Chowdhury, S. U. M. B., Karmakar, A., Chowdhury, N. U. M. K., Moontahab, A., Albin, E. H. C., & Chowdhury, K. A. (2025). Role of tropical cyclone heat potential in the intensification of super cyclone Amphan and its impact on dissolved oxygen dynamics in the Bay of Bengal. *Natural Hazards*. Advance online publication. https://doi.org/10.1007/s11069-025-07567-8

[26] Kabir, M., Chowdhury, M. S., Sultana, N., Jamal, M. S., & Techato, K. (2022). Ocean renewable energy and its prospect for developing economies. In I. Khan (Ed.), *Renewable energy*

and sustainability: Prospects in the developing economies (pp. 263–298). Elsevier. https://doi.org/10.1016/B978-0-323-88668-0.00007-3

[27] Asmelash, E., Prakash, G., Gorini, R., & Gielen, D. (2020). Role of IRENA for global transition to 100% renewable energy. In T. S. Uyar (Ed.), *Accelerating the transition to a 100% renewable energy era* (pp. 51–71). Springer International Publishing. https://doi.org/10.1007/978-3-030-40738-4_2

[28] Baptista, L. B., Schaeffer, R., van Soest, H. L., Fragkos, P., Rochedo, P. R., van Vuuren, D., …, & Qimin, C. (2022). Good practice policies to bridge the emissions gap in key countries. *Global Environmental Change*, *73*, 102472. https://doi.org/10.1016/j.gloenvcha.2022.102472

[29] Ibrahim, I. A., Ötvös, T., Gilmanova, A., Rocca, E., Ghanem, C., & Wanat, M. (2021). International Energy Agency. Netherlands: Wolters Kluwer.

[30] Horzela-Miś, A., & Semrau, J. (2025). The role of renewable energy and storage technologies in sustainable development: Simulation in the construction industry. *Frontiers in Energy Research*, *13*, 1540423. https://doi.org/10.3389/fenrg.2025.1540423

[31] Fahim, K. E., de Silva, L. C., Hussain, F., Shezan, S. A., & Yassin, H. (2023). An evaluation of ASEAN renewable energy path to carbon neutrality. *Sustainability*, *15*(8), 6961. https://doi.org/10.3390/su15086961

[32] Ahmad, S. S., Al Rashid, A., Raza, S. A., Zaidi, A. A., Khan, S. Z., & Koç, M. (2022). Feasibility analysis of wind energy potential along the coastline of Pakistan. *Ain Shams Engineering Journal*, *13*(1), 101542. https://doi.org/10.1016/j.asej.2021.07.001

[33] Samal, R. K. (2023). Techno-economic analysis and wind resource assessment for Odisha, India using reanalysis and 80 m mast measurements: A preliminary assessment for policy-makers. *International Journal of Ambient Energy*, *44*(1), 564–577. https://doi.org/10.1080/01430750.2022.2137581

[34] Kaganzi, K. R., Cuni-Sanchez, A., Mcharazo, F., Martin, E. H., Marchant, R. A., & Thorn, J. P. (2021). Local perceptions of climate change and adaptation responses from two mountain regions in Tanzania. *Land*, *10*(10), 999. https://doi.org/10.3390/land10100999

[35] Rahman, M. M., & Alam, K. (2021). Clean energy, population density, urbanization and environmental pollution nexus: Evidence from Bangladesh. *Renewable Energy*, *172*, 1063–1072. https://doi.org/10.1016/j.renene.2021.03.103

[36] World Health Organization. (2023). WHO Malaria Policy Advisory Group (MPAG) meeting report, 18–20 April 2023. https://www.who.int/publications/i/item/9789240074385

[37] Lewis, C. T. (2022). Climate change and the Caribbean: Challenges and vulnerabilities in building resilience to tropical cyclones. *Climate*, *10*(11), 178. https://doi.org/10.3390/cli10110178

[38] Omondi, O. A., & Lin, Z. (2023). Trend and spatial–temporal variation of drought characteristics over equatorial East Africa during the last 120 years. *Frontiers in Earth Science*, *10*, 1064940. https://doi.org/10.3389/feart.2022.1064940

[39] Xiao, M., & Cui, Y. (2021). Source of evaporation for the seasonal precipitation in the Pearl River Delta, China. *Water Resources Research*, *57*(8), e2020WR028564. https://doi.org/10.1029/2020WR028564

[40] Lagmay, A. M. F., Bagtasa, G., Andal, D. F., Andal, F. D., Aldea, J., Bencito, D. C., …, & Delmendo, P. A. (2024). An impact-based flood forecasting system for citizen empowerment. *Asian Journal of Agriculture and Development*, *21*, 129–148. https://doi.org/10.22004/ag.econ.348355

[41] Ferreira Nogueira, D. (2019). Mobile-based Early warning systems in Mozambique: An exploratory study on the viability to integrate cell broadcast into disaster mitigation routines.

[42] Chari, F., & Novukela, C. (2023). The influence of information and communication technologies on disaster relief operations: A case of Cyclone Idai in Zimbabwe. *Journal of Humanitarian Logistics and Supply Chain Management*, *13*(4), 399–409. https://doi.org/10.1108/JHLSCM-11-2021-0119

How to Cite: Babar Chowdhury, S. U. M., Karmakar, A., Azam Chowdhury, K. M., Tahsin, T. H., Al Mamun Siddiqui, A., Khan, T. S., & Uddin, M. R. (2025). Spatiotemporal Variations and Trends of Atmospheric Parameters Influencing Coastal Resilience in Cox's Bazar, Bangladesh. *Remote Sensing for Sustainable Oceans*. https://doi.org/10.47852/bonviewRSSO52026547

AUTHOR QUERY FORM

Author queries that require author intervention (kindly delete this section once all queries have been addressed):

AQ #	Query	Answer
AQ1	The sentence that starts with "$\sum_{i=1}^{N} \boldsymbol{PC}(\boldsymbol{t}_i)$ was used to" was edited for clarity and conciseness. Please check if appropriate.	